

# DEVELOPMENT OF NOVEL FUNCTIONAL THIN FILMS FOR PHOTONIC DEVICES

A dissertation submitted to



DEPARTMENT OF ELECTRONICS & COMPUTING  
GRADUATE SCHOOL OF ENGINEERING  
GUNMA UNIVERSITY, KIRYU, JAPAN  
(群馬大学大学院工学研究科工学専攻電子情報工学領域)

In partial fulfillment for the award of

**Doctor of Philosophy**

Submitted By:

**MAYANK KUMAR SINGH**

Department of Electronics & Computing  
Gunma University, Kiryu, Japan  
March 2010

Under the supervision of

**Prof. O. Hanaizumi**

Department of Electronics & Computing  
Gunma University, Kiryu, Japan

*Dedicated to*


*All Professionals in Photonics Research*

*Who spend their lives  
exploring the shifting landscape of  
Light*

*And  
My Grand Parents*

*“Let noble thoughts come to us from every side”*

*Vedas*



# CERTIFICATE

*This is to certify that this dissertation entitled, “Development of novel functional thin films for photonic devices”, by Mayank Kumar Singh for the award of “Doctor of Philosophy” degree, comprises of bonafide work done by him at the Department of Electronics & Computing, Gunma University, Kiryu, Gunma, Japan from April’ 2006 to March’ 2010, under my supervision and guidance and to my full satisfaction.*

*I recommend this piece of work for acceptance as project for the partial fulfillment of the degree of “Doctor of Philosophy” of the Department of Electronics & Computing, Gunma University for the year March’ 2010.*

*Date:*

*Prof. O. Hanaizumi*

*Department of Electronics & Computing  
Gunma University, Kiryu, Japan*

## *Acknowledgements*

*Each of us is a reflection of our own knowledge and experience, but the influence of others is indispensable. I hereby acknowledge with gratitude and affection all those who have helped me in the completion of this dissertation work, and in particular:*

*First and foremost I would like to thank to my supervisor **Prof. O. Hanaizumi**, Department of Electronics & Computing, Gunma University, for his encouragement, valuable advice and timely guidance during the entire course of this study. I am thankful to him for providing me the opportunities that were very crucial for bringing the initial ideas to the completed form. I will always remain indebted to him for his support and inspiration.*

*Also I would like to extend my gratitude to Associate **Prof. K. Miura**, Department of Electronics & Computing, Gunma University, for his cooperation in experimental work and valuable feedback.*

*I would like to express my gratitude to **Prof. M. Ito**, **Prof. H. Sakurai**, **Prof. T. Nagao**, and **Prof. M. Takahashi**, for their valuable feedback and suggestions on my research.*

*I am thankful to **Prof. K. Takada**, **Prof. S. Adaichi**, and **Prof. M. Takahashi**, Faculty of Engineering for their useful lectures and discussion.*

*I would like to thank Prof. H.K.Dixit from J.K.Institute, Allahabad, India, Prof. M.S.Tiwari, Prof. Arvind Tripathi and Prof. R.K.Soni from S.G.S.College, Sidhi, India for their support during my studies and research work,*

*I would like to thank my colleagues and associates at Department of Electronics Engineering, Gunma University, who stayed with me till the end. This work would not have been possible without their involvement, for which I will always remain grateful. Thanks to Dr. Jaspal Bange, Umenyi Amarachukwu Velentine, K. Kano, Y. Machida, G. Fusegi, and Lee, for their support.*

*I am also thankful to my colleagues Dr. Ramgopal Gangwar and Abhinay Sharma at J.K.Institute, India for their support during my research work at J.K.Institute, Allahabad, India.*

*I would like to express my gratitude to Department of Electronics & Computing, Gunma University, for providing me a platform to develop my skills and expertise in the subject.*

*Thanks to Student Support Section staff for extending their unflinching support and over-whelming encouragement. I would like to mention the names of Katy Niwa and Emi Fukuda for helping me to survive in Japan with my limited Japanese ability.*

*Thanks to Library Staff at Gunma University, for their valuable help in literature survey.*

*I would like to thank my amazing friends, wonderful people with their irrational and unbreakable belief in me, right from providing honest comments to easing away my tensions, they were always there for me. Mayumi, Miho, Hanbin, and Egemen, thanks for being such a nice friend.*

*Special thank to Barry Keith for his encouraging words and his help in editing my papers.*

*Thanks to my family, for their amazing forbearance, love, and patience, over what has been a very long haul. It is their love and support, which is the basis for everything. I would like to thank to my Mother and Father for their love and trust. I am also thankful to my Uncle Mr. Manoj Kumar for being an inspiration and mentor. I would also like to thank to younger generation of my family for their unconditional support Thanks to Milind, Soniya, Runjhun, Ranu and my beloved wife Seema.*

*Last but not the least, I thank Ministry of Education, Culture, Sports, Science and Technology, Japan (Monbukagakusho) for providing scholarship for my PhD study.*

*Mayank Kumar Singh*

*March' 2010*

*Kiryu, Japan*

## *Preface*

Photonics research is one of the most exciting and challenging research fields of electronics. There is a multitude of factors involved. This thesis involves “**Development of novel functional thin films for photonic devices.**” The research topic chosen represents the fabrication and characterization of thin films fabricated with novel functional materials.

Despite certain limitations, the study tries to address thin film fabrication, characterization, and applications of such thin films in photonic devices and a lot more. It also enables the identification of some of the core issues involved in thin film fabrication with RF-sputtering. The work also highlights the strengths and weaknesses of these films for light emitting devices.

The data collected and the recommendations made can be further used as a tool in assessing the possible application of Er-TaO<sub>x</sub> films for photonic devices, and can also serve as a basis for further research by interested people.

Last but not the least, this thesis is based on the data and information collected during Apr.’ 2006- Mar.’ 2010 and will not be responsible for any changes that may have taken after this period.



## *Table of Contents*

<i>List of Tables</i> .....	XI
<i>List of Figures</i> .....	XII
<i>List of publications</i> .....	XIV
<i>Acronyms</i> .....	XV
<i>Abstract</i> .....	XVIII
<b>1. Introduction</b>	
1.1. Silicon Technology .....	1
1.2. Optical interconnects .....	3
1.3. Silicon light emitters .....	3
1.4. Silicon Nanocrystals .....	5
1.5. Photonic-bandgap materials .....	7
1.6. Alternate materials .....	8
1.7. Outline of this thesis.....	9
Works cited .....	11
<b>2. Erbium Doped Materials</b>	
2.1. Introduction .....	13
2.2. Erbium Doped thin films .....	14
2.3. Er-doped thin films for photonic applications .....	15
2.4. Er-doped light emitters .....	17
2.5. Summary .....	18
Works cited .....	19

### ***3. Erbium Doped Tantalum Pentaoxide***

3.1. Introduction .....	22
3.2. Fabrication of Ta <sub>2</sub> O <sub>5</sub> thin films with various deposition techniques .....	23
3.2.1. Chemical vapor deposition (CVD) .....	24
3.2.2. Sputtering .....	26
3.2.3. Sol-gel method .....	26
3.3. Properties of tantalum pentoxide thin films .....	27
3.3.1. Physical and optical properties .....	27
3.3.2 Structural properties of the crystalline phase .....	28
3.4. Er-Doped tantalum pentoxide films .....	30
3.5. Summary .....	31
Works cited .....	32

### ***4. Experimental Design***

4.1. Introduction .....	40
4.2. Different fabrication techniques .....	40
4.3. RF-sputtering .....	41
4.4. Experimental details of RF-Sputtering system .....	42
4.5. Annealing .....	50
4.6. PL Measurement Setup .....	52
4.7. Electron Probe Micro Analyzer (EPMA) .....	54
4.8. X-Ray Diffraction (XRD) .....	56

4.9. Surface Profiler .....	57
4.10. Spectrophotometer .....	58
Works cited.....	59
<b>5. Results and Discussion</b>	
5.1. Results and Discussion .....	60
Works cited .....	79
<b>6. Summary and conclusion</b>	
6.1. Summary and conclusion .....	81

## *List of Tables*

- Table-3.1. - Physical and optical properties of Ta<sub>2</sub>O<sub>5</sub> thin films for different sample preparation techniques.
- Table-4.1. - Details of sputtering processing condition for SiO<sub>2</sub> / Er<sub>2</sub>O<sub>3</sub> samples
- Table-4.2. - Details of sputtering processing condition for Ta<sub>2</sub>O<sub>5</sub> samples
- Table-4.3. - Details of sputtering processing condition for Ta<sub>2</sub>O<sub>5</sub> / Er<sub>2</sub>O<sub>3</sub> samples
- Table-4.4. - Details of sputtering processing condition for Ta<sub>2</sub>O<sub>5</sub> /Er<sub>2</sub>O<sub>3</sub>, Yb<sub>2</sub>O<sub>3</sub> samples
- Table-5.1. - Annealing temperature V/s band gap
- Table-5.2. - Concentration of Er in different samples measured with EPMA.

## *List of Figures*

- Fig. 1.1. - CPU transistor counts 1971 - 2008
- Fig. 1.2. - Indirect bandgap in Silicon
- Fig. 2.1. - Energy level diagram of  $\text{Er}^{3+}/\text{Yb}^{+3}$  ions
- Fig. 4.1. - Sputtering machine used in film fabrication
- Fig. 4.2. - Schematic diagram of sputtering machine
- Fig. 4.3. - Schematic diagram of sputtering Process
- Fig. 4.4. - Target Setup for sputtering
- Fig. 4.5. - KDF-S70 Electric Furnace
- Fig. 4.6. - Heating chamber of KDF-S70 electric furnace
- Fig. 4.7. - Schematic diagram of PL measurement setup
- Fig. 4.8. - PL Measurement Setup
- Fig. 4.9. - Surface Profiler Dektak-II
- Fig. 4.10. - Spectrophotometer Shimadzu MPC-3100
- Fig. 5.1. - PL spectrum of Er-SiO<sub>2</sub> films annealed at different temperatures
- Fig. 5.2. - PL spectrum of Er-SiO<sub>2</sub> films with different Er concentration
- Fig. 5.3. - PL spectrum of Er-SiO<sub>2</sub> films with different film thickness
- Fig. 5.4. - Transmittance spectra of samples
- Fig. 5.5. - Photon energy V/s absorption coefficient
- Fig. 5.6. - PL spectra of Ta-oxide films after annealing at 600,700 and 800°C

- Fig. 5.7. - Visible light emission from Tantalum pentaoxide film annealed at 700°C
- Fig. 5.8. - PL Spectra of samples annealed for 20, 30 and 40 min.
- Fig. 5.9. - PL spectra of samples fabricated with different RF power
- Fig. 5.10. - PL spectra of samples fabricated with different Ar pressure
- Fig. 5.11. - PL spectra of Er-TaOx films annealed at 600 to 1100°C for 20 min.
- Fig. 5.12. - PL spectra of samples annealed at 900°C for 10 - 40 min
- Fig. 5.13. - PL spectra of samples with different Er concentrations (mol %) annealed at 900°C for 20 min.
- Fig. 5.14. - XRD patterns of the films annealed at various temperatures.
- Fig. 5.15. - XRD patterns of the films annealed from 10 to 40 min.
- Fig. 5.16. - XRD patterns of the films fabricated with different Er concentration.
- Fig. 5.17. - Green light emission from Er-TaOx films.
- Fig. 5.18. - PL spectra of samples with different Er-Yb concentrations annealed at different temperature for 20 min.
- Fig. 5.19. - PL spectra of samples annealed at different temperatures for 20 min.

## *List of Publications*

- “Intense photoluminescence from erbium-doped tantalum oxide thin films deposited by sputtering”, M. K. Singh, G. Fusegi, K. Kano, J. P. Bange, K. Miura, and O. Hanaizumi, IEICE Electronics Express, Vol.6, No.23, pp1676-1682, Dec. 2009.
- “Light emission from Er-doped Ta-oxide films fabricated by RF-sputtering”, M. K. Singh, G. Fusegi, K. Kano, K. Miura, and O. Hanaizumi, ICOM 2009, Montenegro.
- “Structural analysis of RF sputtered Er doped Ta<sub>2</sub>O<sub>5</sub> films”, J. P. Bange, M. K. Singh, G. Fusegi, K. Kano, K. Miura, and O. Hanaizumi, AMDE 2009, Japan
- “Light-emitting properties of Er-doped TaOx thin films fabricated by using RF sputtering”, K. Miura, K. Kano, G. Fusegi, M. K. Singh, and O. Hanaizumi, IEICE Tech. Rep., vol. 109, no. 175, OPE2009-101, pp. 141-144, Aug. 2009.
- “Visible-light emission properties of Er:TaOx thin films fabricated by using RF sputtering”, K. Miura, K. Kano, G. Fusegi, M. K. Singh, and O. Hanaizumi, JSAP Autumn meeting 2009, Japan.
- “Fabrication and optimization of green light emitting Er-TaOx films”, M. K. Singh, J. P. Bange, G. Fusegi, K. Kano, K. Miura, and O. Hanaizumi, AMDE 2009, Japan
- “Fabrication of light emitting TaOx films by RF sputtering”, K. Miura, K. Kano, G. Fusegi, M. K. Singh, and O. Hanaizumi, AMDE 2009, Japan

## *Acronyms*

Å	Angstrom
ALD	Atomic layer deposition
ALE	Atomic layer epitaxy
AMDE	Advanced micro device engineering
ATEC	Advance Technology and Education Center, Gunma University
CCD	Charge-coupled device
CVD	Chemical vapor deposition
DRAM	Dynamic random access memory
EDFA	Erbium doped fiber amplifier
EPMA	Electron microprobe analyzer
Er	Erbium
Er <sub>2</sub> O <sub>3</sub>	Erbium oxide
Er-SiO <sub>2</sub>	Erbium-doped silicon dioxide
eV	Electron volt
GaAs	Gallium Arsenide
GeO <sub>2</sub>	Germanium oxide
h	Planck constant
ICOM	International conference on physics of materials
InGaAsP/InP	Indium Gallium Arsenide phosphide / Indium phosphide
IR	Infrared Radiation
ITRS	International Technology Roadmap for Semiconductors



keV	Kilo electron volt
LiNbO <sub>3</sub>	Lithium niobate
LPCVD	Low-pressure chemical vapor deposition
Mol%	Molecular percentage
NC	Nanocrystal
Pa	Pascal
PBG	Photonic band gap
PECVD	Plasma-enhanced chemical vapor deposition
PL	Photoluminescence
PVD	Physical vapor deposition
RF	Radio frequency
sccm	Standard cubic centimeter
SEM	Scanning electron microscope
SiO <sub>2</sub>	Silicon dioxide
Si NC	Silicon nanocrystal
Si <sub>3</sub> N <sub>4</sub>	Silicon nitride
TaO <sub>x</sub>	Tantalum Oxide
Ta <sub>2</sub> O <sub>5</sub>	Tantalum pentoxide
Ti	Titanium
WDM	Wave length division multiplexing
XRD	X-ray Diffraction
Yb	Ytterbium

$\text{Yb}_2\text{O}_3$	Ytterbium oxide
3D	Three dimensional
$\beta\text{-Ta}_2\text{O}_5$	Beta tantalum pentoxide
$\mu\text{m}$	Micrometer

## *Abstract*

Rare-earth doped thin films are drawing increasing attention for their use in amplifiers and lasers and their suitability for integrated optics. The optical properties of rare-earth ions in solids have been investigated widely and are well understood. Er<sup>3+</sup>-doped materials are attracting much attention because of the search for solid-state-laser devices operating in the green region, optical devices for 3D displays and for waveguides, which can work in telecommunication window.

In this dissertation we researched and fabricated different novel functional thin films for photonics devices fabricated by RF-magnetron sputtering method as –

- **Erbium-doped SiO<sub>2</sub>**
- **Tantalum pentoxide [Ta<sub>2</sub>O<sub>5</sub>]**
- **Erbium-doped Tantalum pentoxide [Er-TaO<sub>x</sub>]**
- **Erbium- Ytterbium co-doped Tantalum pentoxide**

We fabricated different thin films using the RF-sputtering method and then annealed them at various temperatures and time durations. PL peaks were observed at wavelengths of 550 and 670 nm from the Er-TaO<sub>x</sub> films. We observed the strongest intensities of the 550 and 670 nm peaks from the samples with 0.96 and 0.63 mol% Er concentrations after annealing at 900° C for 20 min, respectively. To the best of our knowledge, this is the first report of light emission from Er-TaO<sub>x</sub> films fabricated by the RF-sputtering method. These results demonstrate that Er-TaO<sub>x</sub> films fabricated by RF sputtering can serve as high quality luminescent layers.

These can easily be combined with other passive devices to realize novel active devices (e.g., a green-light-emitting photonic crystal), as only sputtering and annealing processes are needed for fabrication.

Recent reports of optical waveguides fabricated on Ta<sub>2</sub>O<sub>5</sub>, higher nonlinear susceptibility  $\chi^3$  of Ta<sub>2</sub>O<sub>5</sub>, and light emission from thin films makes Ta<sub>2</sub>O<sub>5</sub> a promising material for novel photonic devices.

**CHAPTER - 1**

**INTRODUCTION**



## Chapter 1

### *Introduction*

---

The complexity for minimum component costs has increased at a rate of roughly a factor of two per year . . . , this rate can be expected to continue . . . [1.1]

International Technology Roadmap for Semiconductors (ITRS), a public document prepared every other year by a consortium representing the global semiconductor industry [1.2]. The roadmap is intended “to provide a reference of requirements, potential solutions, and their timing for the semiconductor industry” over a fifteen-year horizon. For many years, the ITRS has highlighted one threat to continued scaling in particular that must be addressed in the short term future in order to avoid slowing down the pace of Moore’s Law (Fig. 1.1).

Increasing processor speed has resulted in larger number of gates on the chip die. We tend to see larger processors as more efficient methods of integrating larger number of transistors. But due to the interconnect bottleneck there would be a certain upper limit to which we could go.

Metallic interconnects on chip are typically associated with high time constants and add to the overheads when it comes to optimizing for high clock speeds. With increasing component density on chip there would even be a need to have faster

Interconnect between the devices to still enable single clock operation on the chip. Optical interconnects might be a solution for the scaling process in silicon electronics.

## **1.2. Optical interconnects**

Optical interconnects are essential for continued scaling progress in silicon electronics, they can open an enormous market for integrated photonic circuit technology. Optical interconnects can give a new direction and future to photonics technology. Novel products can be made possible by the widespread availability of affordable, high-density optical systems. Considering the historical development of computing hardware from the relays and vacuum tubes of early telephone networks, it is possible that optical interconnects could someday lead to all-optical computers, perhaps including systems capable of quantum computation [1.3, 1.4]. Unfortunately, there is at present no clear path to practical on-chip optical data transfer and scalable all-photonic integrated circuits. The obstacles that currently stand in the way of optical interconnects are challenges for device physics and materials science. Breakthroughs are needed that either improve the set of materials available for micro photonic devices or obviate the need for increased materials performance through novel device designs. Light emission from silicon is a hindrance on the way to optical interconnect.

## **1.3. Silicon light emitters**

Silicon is not an appropriate material for light emitting devices, including lasers, due to its indirect band structure (Fig.1.2. adapted from Havard.edu). This means that the least energetic conduction band electrons in silicon are in motion relative to the most energetic valence band electron states. In order for silicon to absorb or emit a photon at visible frequencies, an electron must undergo a band-to-band transition between two of these states. This transition requires the simultaneous absorption or emission of a phonon (the quantum of lattice vibration) in order to accommodate the momentum mismatch, making it much less likely to occur.



**Chapter 1**  
*Introduction*

---

Because a radiative transition is unlikely, competing nonradiative recombination channels tend to dominate the relaxation of the excited state electrons. Ultimately this makes photon emission in silicon extremely inefficient ( $10^{-7} - 10^{-4}$ ) unless great efforts are made to purify the material and to passivate all surfaces [1.5]. The recently reported “first silicon laser” [1.6, 1.7] did not rely on the emission of photons by excited conduction band electrons. Instead it is operated by Raman scattering, in which sub-bandgap photons interact only with phonons.

The crystallinity of silicon makes Raman scattering relatively strong in relation to amorphous glasses, but intense optical pumping is still required to create a population inversion of the excited virtual phonon state.

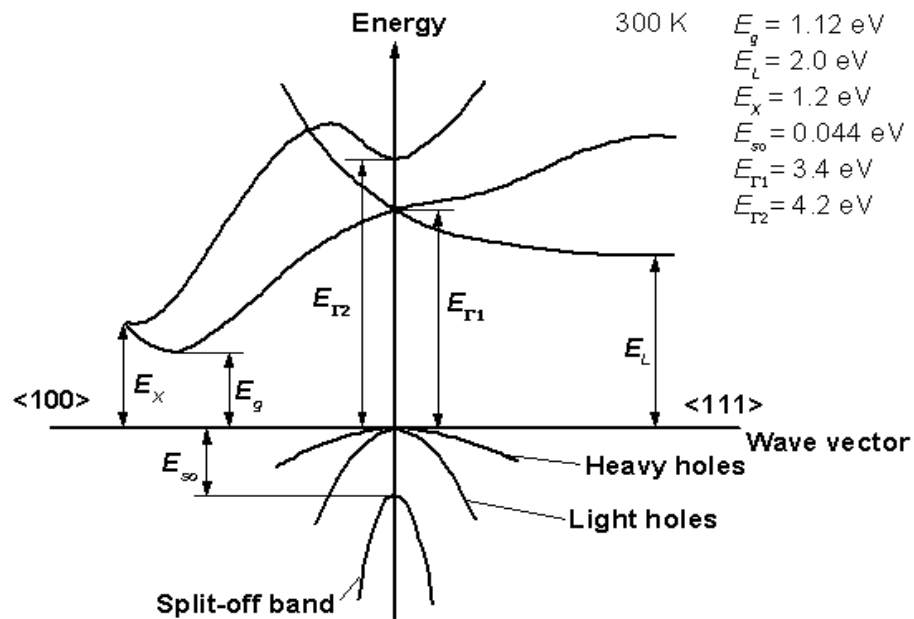


**Fig.1.2. Indirect bandgap in Silicon**

Under such intense illumination, simultaneous two-photon absorption excites electrons into the conduction band, which can then attenuate the laser signal through free carrier absorption. The subsequent “first continuous silicon laser” was achieved through better management of these free carriers [1.8]. While these results are impressive, it is clear that Raman lasers do not have a practical future because they require optical excitation by a pump laser and have a relatively small spectral range in which gain can be achieved [1.9].

Light emission from silicon is one of the most challenging problems in photonics research. There are many different approaches and efforts to get light emission from silicon as-

- Silicon Nanocrystals
- Photonic-bandgap materials
- Alternate materials

#### **1.4. Silicon Nanocrystals**

The first approach to fabricate silicon light emitter was reported with silicon nanocrystals. Light emission reported by L. Pavesi [1.10], attracted great attention. Silicon nanocrystals could be a possible solution because of their tunable indirect bandgap and more efficient electron-hole recombination.

There are two factors that contribute to improvement in the radiative recombination rate in silicon nanocrystals. The first can be understood in the context of Fermi’s Golden Rule for quantum mechanical transitions, which can be derived using time dependent perturbation theory. In the formalism of Fermi’s Golden Rule, the rate of

## Chapter 1

### *Introduction*

---

an optical dipole transition is proportional to the magnitude of an off-diagonal matrix element calculated by evaluating an overlap integral that connects the electron and hole wave functions together through the dipole operator. Because the nanocrystals form a potential well that confines the electron and the hole spatially, these wave functions overlap more in position space and the matrix element, or oscillator strength, for the transition increases [1.11].

At the same time, the uncertainty in momentum space that confinement introduces relaxes the momentum conservation rule and allows a greater proportion of the phonon density of states to assist in the indirect band-to-band transition [1.12].

This effect is thought to be insufficient to make the bandgap of silicon nanocrystals direct but the optical transitions in small nanocrystals might possibly be described as quasidirect. Reports claiming direct gap transitions in silicon nanocrystals at blue emission wavelengths on the basis of decay rate measurements are likely to correspond to misattributed radiative emission from oxide defect centers or to fast nonradiative recombination [1.13 - 1.15].

Therefore, it is found that due to quantum confinement the direct bandgap decreases. In combination with the phonon bottleneck effect, which slows down carrier cooling by phonon emission and thereby increases the probability of direct recombination for smaller NCs, this tunable direct bandgap offers new possibilities for efficient and tunable light emission from Si NCs. In addition, the decrease of the direct bandgap gives rise to a higher absorption, which is beneficial for Si NC solar cells.

While silicon nanocrystals alone cannot emit light in the infrared telecom bands, they can be coupled to the emission of erbium ions to create a promising hybrid optical material.

### **1.5. Photonic-bandgap materials**

The second major hope for silicon light emitter is from photonic-bandgap materials. In its intrinsic form, silicon has an indirect electronic bandgap with an optical absorption edge in the near infrared (IR) at 1.05  $\mu\text{m}$ . Because of the indirect character of the bulk form of silicon it only emits light very weakly. This makes the bulk form most useful for microelectronic but not for optoelectronic applications where efficient light emission from silicon is needed. To evoke efficient light emission from silicon, nano-scale structures smaller than the bulk exciton are required. At this length scale, spatial and quantum confinement effects enhance the chances of radiative over non-radiative electron hole recombination processes and luminescence can be seen from photolytically or electrically stimulated silicon [1.16].

The idea of novel all-optical devices, i.e. switches, modulators, filters and interconnects, seems to be possible with photonic-bandgap materials: materials patterned with a periodicity in the dielectric constant, which generates a range of “forbidden” frequencies, called photonic bandgap. Photons with energies within this bandgap cannot propagate through the material. This will allow controlling and manipulating the propagation of light even within compact systems of very small dimensions. In a photonic band gap (PBG), lasing can occur with zero pumping thresholds. Lasing can also occur without mirrors and without a cavity mode since each atom creates its own localized photon mode. This suggests that large arrays of

nearly lossless micro-lasers for all-optical circuits can be fabricated with PBG materials.

### **1.6. Alternate materials**

There are various approaches to develop alternate materials for silicon light emitter. Gallium Arsenide (GaAs) has been suggested as an alternate material for some time. Prime advantage of GaAs is that it has a direct band gap, which means that it can be used to emit light efficiently. Silicon has an indirect bandgap and so is very poor at emitting light. As a wide direct band gap material with high breakdown voltage, and resulting resistance to radiation damage, GaAs is an excellent material for optical windows in high power applications. However, the lack of a native oxide, high processing cost and environmental concerns discourage the industry from implementing GaAs as a feasible solution.

Although several III-V group materials emit in the **1.33-1.55**  $\mu\text{m}$  range, the InGaAsP/InP material system is highly developed. The commonly used light-emitter in the region of 1.3  $\mu\text{m}$  lasers is  $\text{In}_{0.74}\text{Ga}_{0.26}\text{As}_{0.6}\text{P}_{0.4}$ , whereas for 1.55  $\mu\text{m}$  devices, it is  $\text{In}_{0.6}\text{Ga}_{0.4}\text{As}_{0.9}\text{P}_{0.1}$ . For optoelectronic GaInAsP-InP DH lasers, LPE, VPE and LPMOVPE (low pressure-MOVPE) are potentially useful for the growth of high quality DH lasers emitting between 1.2 and 1.6  $\mu\text{m}$ . Difficulties have been reported with the growth of phosphorus-bearing alloys by MBE. However, the results obtained clearly demonstrated that high quality InGaAsP/InP materials suitable for the state-of-the-art device applications could be routinely prepared by CBE [1.17].

### **1.7. Outline of this thesis**

This thesis presents experimental work of developing functional thin films with novel optical material for applications in silicon photonics devices. The chapters are organized as follows:

In chapter 2, we discuss Er-doped materials. First we discuss energy diagram of  $\text{Er}^{3+}/\text{Yb}^{+3}$  ions and their possible up-conversion; next topic covers thin films fabricated with Er-doped materials and application of such thin films in photonic devices. In the next topic of the chapter we discuss Er-doped thin films for waveguide applications fabricated with different host materials. In the last topic we discuss about the different approaches for Er-doped light emitters.

Chapter 3 presents the fabrication and application of erbium doped tantalum pentoxide material. We did a comparative study of various deposition techniques for fabrication of  $\text{Ta}_2\text{O}_5$  thin films, on the basis of their advantages and disadvantages. The next topic deals with the physical, optical, and structural properties of  $\text{Ta}_2\text{O}_5$ . In next topic we discuss about the fabrication and applications of Er-doped tantalum pentoxide films.

Chapter 4 describes the experimental design for fabrication and characterization of thin films used in this dissertation. First, we discuss about different fabrication techniques available for thin film deposition. Next topic gives the detail about experimental setup of RF-sputtering machine and other details. Details of RF-sputtering conditions for fabrication of thin films with different materials are also presented in tables in this part. Details of annealing furnace, PL measurement setup,

## **Chapter 1**

### ***Introduction***

---

EPMA, X-ray diffraction, surface profiler, spectrophotometer used in this dissertation also presented in this chapter.

Chapter 5 presents the results and discussion of the experiments carried out in this dissertation. First, we presented various experimental results as - PL spectra of different samples fabricated with different functional materials, XRD spectra of various thin films, EPMA results of thin films. Discussion is followed by experimental results.

Chapter 6 describes the conclusion of this dissertation and direction for future works.

**WORKS CITED**

- 1.1. Gordon E. Moore, "Cramming more components onto integrated circuits" *Electronics*, Vol. 38, No. 8, 1965.
- 1.2. International Technology Roadmap for Semiconductors (ITRS) <http://itrs.net/>.
- 1.3. A. Steane, *Rep. Prog. Phys.* Vol.61, pp117, 1998.
- 1.4. E. Knill, R. Laflamme, and G. J. Milburn, *Nature*, vol.409, pp46, 2001.
- 1.5. M. A. Green, J. Zhao, A. Wang, P. J. Reece, and M. Gal, *Nature*, vol.412, pp805, 2001.
- 1.6. O. Boyraz, B. Jalali, *Optics Express*, vol.12, pp5269, 2004.
- 1.7. H. Rong, A. Liu, R. Jones, O. Cohen, D. Hak, R. Nicolaescu, A. Fang, and M. Paniccia, *Nature*, vol.433, pp292, 2005.
- 1.8. H. Rong, R. Jones, A. Liu, O. Cohen, D. Hak, A. Fang, and M. Paniccia, *Nature*, vol.433, pp725, 2005.
- 1.9. Silicon Nanocrystals for Silicon Photonic PhD thesis by Robert Joseph Walters, California Institute of Technology Pasadena, California, 2007.
- 1.10. L. Pavesi, L. Dal Negro, C. Mazzoleni, G. Franzo, and F. Priolo, *Nature*, vol.408, pp440, 2000
- 1.11. B. Delley and E. F. Steigmeier, *Phys. Rev. B* 47, pp13970, 1993.
- 1.12. D. Kovalev, H. Heckler, M. Ben-Chorin, M. Schwartzkopf, and F. Koch, *Phys. Rev. Lett.* 81, pp2803, 1998.
- 1.13. G. Belomoin, J. Therrien, and M. Nayfeh, *Appl. Phys. Lett.* 77, pp779, 2000.
- 1.14. M. H. Nayfeh, N. Barry, J. Therrien, O. Akcakir, E. Gratton, and G. Belomoin, *Appl. Phys. Lett.* 78, pp1131, 2001.
- 1.15. A. Smith, Z. H. Yamani, N. Roberts, J. Turner, S. R. Habbal, S. Granick, and M. H. Nayfeh, *Phys. Rev. B* 72, pp205307, 2005.



## **Chapter 1**

### ***Introduction***

---

- 1.16. Emmanuel Chomski and Geoffrey A. Ozin, Panoscopic Silicon - A material for all length scales, *Adv. Mater.*, 12, No. 14, 2000.
- 1.17. Mohamed Henini, Semiconductor lasers: An overview part II, III-Vs Review, Vol. 6, Issue 5, pp50-53, 1993.

**CHAPTER - 2**

**ERBIUM DOPED**

**MATERIALS**

## 2.1. Introduction

Erbium is a rare earth element belongs to the group of the Lanthanides. When embedded in a solid, erbium generally assumes the trivalent  $\text{Er}^{3+}$  state, which has an electronic configuration  $[\text{Xe}]-4f$ . Fig.2.1. Shows energy diagram of  $\text{Er}^{3+}$  and their corresponding transitions. The Er-ion has an incompletely filled  $4f$ -shell, allowing for different electronic configurations with different energies due to spin - spin and spin-orbit interactions. Radiative transitions between most of these energy levels are parity forbidden for free  $\text{Er}^{3+}$  ions. When Er is incorporated in a solid however, the surrounding material perturbs the  $4f$  wave functions. This has two important consequences. First, the host material can introduce odd-parity character in the Er  $4f$  wave functions, making radiative transitions weakly allowed.

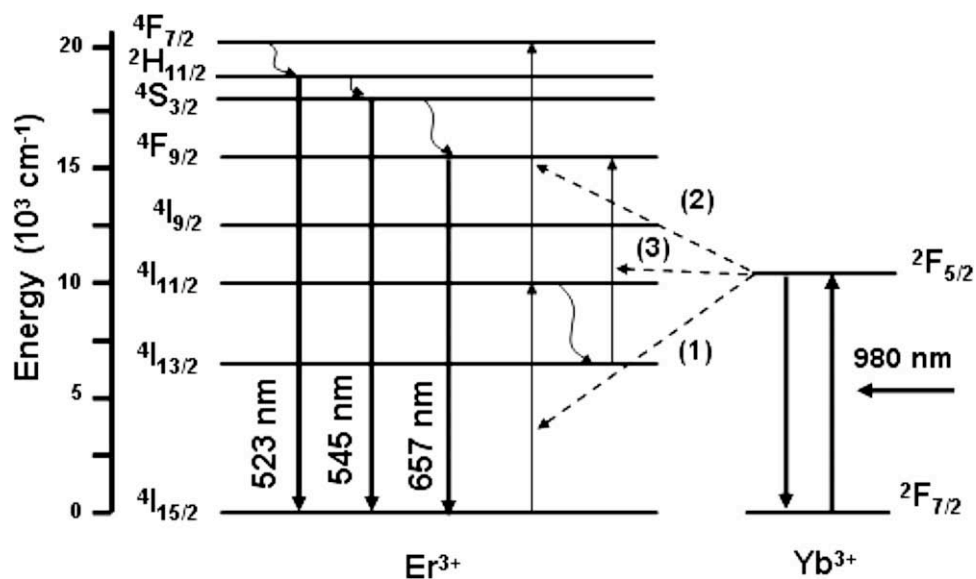


**Fig. 2.1 Energy level diagram of  $\text{Er}^{3+}/\text{Yb}^{3+}$  ions and possible up-conversion luminescence mechanisms [Adapted from ref. 2.1].**

Second, the host material causes Stark-splitting of the different energy levels, which results in a broadening of the optical transitions. Since radiative transitions in  $\text{Er}^{3+}$  are

only weakly allowed, the cross sections for optical excitation and stimulated emission are quite small, typically on the order of  $10^{-21}$  cm<sup>2</sup>, and the radiative lifetimes of the excited states are long, up to several milliseconds. When Er is excited in one of its higher lying levels it rapidly relaxes to lower energy levels via multi-phonon emission. This results in typical excited state lifetimes ranging from 1 ns to 100 μs. The transition from the first excited state (<sup>4</sup>I<sub>13/2</sub>) to the ground state (<sup>4</sup>I<sub>15/2</sub>) is an exception to this rule. Due to the large transition energy (0.8 eV) multi-phonon emission is unlikely, resulting in lifetimes up to ~20 ms depending on host material, and efficient emission at 1.54 μm [2.2].

## **2.2. Erbium Doped thin films**

Thin film integrated optics is becoming more and more important in optical communications technology. The technology for the fabrication of passive devices such as planar optical waveguides, splitters, and multiplexers is now quite well developed, and devices based on this technology are now commercially available. Next step to further improve this technology is to develop optical amplifiers that can be integrated with these devices. Such amplifiers can serve to compensate for the losses in e.g. splitters or other components, and can also serve as preamplifiers for active devices such as detectors.

Erbium doped materials have attracted much attention after the invention of Erbium doped fiber amplifier (EDFAs) in 1987 due to 4*f* emission at telecommunication wavelength. Er<sup>3+</sup> the preferred bonding state has an incomplete 4*f* electronic shell that is covered by closed 5s and 5p shells [2.3]. As a result, rather sharp optical intra-4*f* transitions can be achieved from erbium-doped materials. The transition from the first-excited state to the ground state in Er<sup>3+</sup> occurs at 0.8 eV, corresponding to 1.54

## Chapter 2

### *Erbium Doped Materials*

---

$\mu\text{m}$  wavelength. This is an important telecommunication wavelength since standard silica-based optical fibers have their maximum transparency at this wavelength.

In optical fiber technology, erbium doped fiber amplifiers are now commercially used in long distance fiber communications links. They use an optical transition in  $\text{Er}^{3+}$  at a wavelength of  $1.54 \mu\text{m}$  for signal amplification, and their success has set a standard of optical communication at this wavelength. To use the same concept of Er doping for planar waveguide amplifiers are now being developed. For these devices silicon is often used as a substrate, so that opto-electronic integration with other devices in or on Si (electrical devices, or Si based light sources, detectors, modulators) may become possible.

Erbium doped materials also have great possibilities in thin film integrated optoelectronic technology, due to their emission at  $1.54 \mu\text{m}$  (standard telecommunication wavelength). Er-doped dielectric thin films can be used to fabricate planar optical amplifiers or lasers that can be integrated with other devices on the same chip. Semiconductors, such as silicon, can also be doped with erbium. In this case the Er may be excited through optically or electrically generated charge carriers. Er-doped Si light-emitting diodes may find applications in Si-based optoelectronic circuits [2.4].

### **2.3. Er-doped thin films for photonic applications**

There are many efforts for developing new materials for thin film photonic application.  $\text{LiNbO}_3$  is a key material in integrated optics due to its excellent nonlinear optical properties.

Optical switches and modulators have been made in  $\text{LiNbO}_3$  and are commercially available. Rare-earth-doped waveguide amplifiers in  $\text{LiNbO}_3$  could be used to

## Chapter 2

### *Erbium Doped Materials*

---

compensate for the intrinsic optical losses in such splitters and modulators. In addition, the electro-optical properties can be used to fabricate rare-earth-doped mode-locked, Q-switched, or tunable waveguide lasers [2.5,2.6]. Planar and channel waveguides can be made in LiNbO<sub>3</sub> by Ti indiffusion or proton exchange, and they show optical losses as low as 0.1 – 0.2 dB/cm [2.6].

Buchal et al. first reported Er implantation of LiNbO<sub>3</sub> for optical devices. Optical amplification was demonstrated on single mode Ti-diffused channel waveguides, fabricated on a 300 keV Er-implanted and annealed LiNbO<sub>3</sub> wafer [2.7]. They also made careful studies of the diffusion of Er implanted in LiNbO<sub>3</sub> [2.8]. These studies were later used in the optimization of Er-indiffused LiNbO<sub>3</sub> waveguide lasers.

Researchers also tried other materials implanted with various rare-earth ions:

- Nd-implanted SrTiO<sub>3</sub> showed characteristic photoluminescence of Nd<sup>3+</sup> at 1.05 - 1.08 μm [2.9]
- Tb-implanted Y<sub>3</sub>Al<sub>5</sub>O<sub>12</sub> YAG showed cathode-luminescence at 544, 590, and 620 nm [2.10].
- Sapphire single crystals implanted with Eu showed photoluminescence at 622 nm, particularly after additional laser annealing.
- Si<sub>3</sub>N<sub>4</sub> thin films were also doped with Er by ion implantation [2.11]. This material has a relatively high refractive index (n=1.97), and therefore waveguides with small dimensions and highly confined optical modes can be fabricated. PL from Er<sup>3+</sup> was observed after annealing and had luminescence lifetimes at 1.54 μm of 7 ms at low Er concentration.
- Combined Er and Yb implantations were performed into silicon oxynitride waveguides. In such co-doped waveguides, the aim is to take advantage of the

relatively high absorption cross section of the  $\text{Yb}^{3+}$  ion, which can then resonantly transfer its energy to  $\text{Er}^{3+}$  [2.12].

#### **2.4. Er-doped light emitters**

The origin of the room-temperature photoluminescence (PL) from Si-NCs is still under active debate, and some essential features of this PL signal are still not understood in detail. Several mechanisms have been suggested to explain the appearance of this luminescence signal, such as defects within the  $\text{SiO}_2$  [2.13, 2.14] or at the nanocrystals surface, [2.15-2.18] the formation of siloxane, [2.19-2.21] or quantum-confinement effects of the excitons caused by their spatial confinement within the Si- NCs [2.22-2.24]. For porous silicon, the latter mechanism was proved to be the origin of the observed luminescence by the appearance of silicon phonon-related structures in the resonantly excited PL signal [2.22, 2.24]. For Si-NC within an oxide matrix, this discussion is still ongoing and the answer might be different for different sample systems. Even if, one assumes that quantum confinement is the origin of this luminescence band, this effect could not easily be separated from other effects such as the migration of excitons [2.25-2.28] due to the broad size distribution of the Si-NCs involved.

The situation can become better if one uses the Si-NCs as sensitizers for other active elements, such as  $\text{Er}^{3+}$  ions. The  $\text{Er}^{3+}$  luminescence at  $1.54 \mu\text{m}$  is of great technological interest due to the absorption minimum of  $\text{SiO}_2$ -glass fibers in this wavelength range. The very small absorption cross-section of erbium prevents effective application of  $\text{Er}^{3+}$  in integrated optoelectronics, and so the use of appropriate sensitizers such as Si-NCs, which can transfer their energy to the  $\text{Er}^{3+}$  ions, is highly desirable. The very effective energy transfer to  $\text{Er}^{3+}$  ions also allows the fabrication of efficient electrically pumped devices. ST Microelectronics reported an

## Chapter 2

### *Erbium Doped Materials*

---

Er/Si-NC LED with 10 % efficiency [2.29]. This device does not utilize any additional control of the crystal size besides the conventional phase separation of bulk SiO<sub>x</sub> layers. A device with a narrow Si-NC size distribution should show an even higher efficiency. This narrow size distribution would also facilitate adjusting the Si-NC (sensitizer) emission wavelength to the absorption levels of Er<sup>3+</sup> [2.30].

#### **2.5. Summary**

Er-doped materials and thin films are of great interest due to their transition in 1.5μm wavelength. Erbium doped waveguide amplifiers; Erbium doped waveguides, Erbium doped light emitters can be realized in near future with increasing research in this field. Er-doped materials could be promising candidate for next generation communication devices.



**WORKS CITED**

- 2.1. F.A. Bomfim, J.R. Martinelli, L.R.P. Kassab, N.U. Wetter, J.J. Neto, J. of non-crystalline solids, vol.354, pp.4755, 2008.
- 2.2. P. G. Kik, Energy transfer in erbium doped optical waveguides based on silicon, PhD thesis, FOM-AMOLF, 2000.
- 2.3. S. Hu fner, “Optical Spectra of Transparent Rare-earth Compounds”, Academic, New York, 1978.
- 2.4. A. Polman, Erbium implanted thin film photonic materials, J. Appl. Phys. 82 (1), 1 1997.
- 2.5. R. Brinkmann, W. Sohler, and H. Suche, Electron. Lett. 27, pp415, 1991.
- 2.6. P. Becker, R. Brinkmann, M. Dinand, W. Sohler, and H. Suche, Appl. Phys. Lett. 61, pp1257, 1992.
- 2.7. Ch. Buchal, R. Brinkmann, W. Sohler, and H. Suche, Mater. Res. Soc. Symp. Proc. 201, pp307, 1991.
- 2.8. Ch. Buchal and S. Mohr, J. Mater. Res. 6, pp134, 1991.
- 2.9. M. G. Tenner, Y. A. R. R. Kessener and M. H. F. Overwijk, Nucl. Instrum. Methods Phys. Res. B 80/81, pp1185, 1993.
- 2.10. N. Can, P. D. Townsend, D. E. Hole, and C. N. Afonso, J. Appl. Phys. 78, pp6737, 1995.
- 2.11. O. Lumholt, G. Grand, H. Bernas, J. Chaumont, and S. Valette, Proceedings of the European Conference on Optical Communication, 1992.
- 2.12. A. V. Chelnokov, J.-M. Lourtioz, Ph. Boucard, H. Bernas, J. Chaumont, and T. Plowman, Electron. Lett. **31**, pp636, 1995.
- 2.13. H. Nishikawa, E. Watanabe, D. Ito, Y. Sakurai, K. Nagasawa, Y. Ohki, J. Appl. Phys., vol.80, pp3513, 1996.

## Chapter 2

### *Erbium Doped Materials*

---

- 2.14. M. Zhu, Y. Han, R. B. Wehrspohn, C. Godet, R. Etemadi, D. Ballutaud, *J. Appl. Phys.*, 83, pp5386, 1998.
- 2.15. F. Koch, V. Petrova-Koch, *J. Non-Cryst. Solids*, pp198, 1996.
- 2.16. Y. Kanemitsu, *Phys. Rev. B: Condens. Matter Mater. Phys.*, vol. 49, pp845, 1994.
- 2.17. Y. Kanemitsu, *Phys. Rev. B: Condens. Matter Mater. Phys.*, vol.53, pp515, 1996.
- 2.18. Y. Kanemitsu, S. Okamoto, *Phys. Rev. B: Condens. Matter Mater. Phys.*, 56, R15, pp561, 1997.
- 2.19. S. Finkbeiner, J. Weber, M. Rosenbauer, M. Stutzmann, *J. Lumin.*, 57, pp231, 1993.
- 2.20. H. D. Fuchs, M. Stutzmann, M. S. Brandt, M. Rosenbauer, J. Weber, A. Breitschwerdt, P. Deµk, M. Cardona, *Phys. Rev. B: Condens. Matter Mater. Phys.*, vol. 48, pp8172, 1993.
- 2.21. M. Stutzmann, M. S. Brandt, M. Rosenbauer, J. Weber, H. D. Fuchs, *Phys. Rev. B: Condens. Matter Mater. Phys.*, vol. 47, pp4806, 1993.
- 2.22. V. Lehmann, U. Gösele, *Appl. Phys. Lett.*, vol. 58, pp856, 1991.
- 2.23. P. D. J. Calcott, K. J. Nash, L. T. Canham, M. J. Kane, D. Brumhead, *J. Phys.: Condens. Matter*, vol. 5, L91, 1993.
- 2.24. D. Kovalev, H. Heckler, G. Polisski, F. Koch, *Phys. Status Solidi B*, vol. 215, pp871, 1999.
- 2.25. L. Pavesi, *J. Appl. Phys.*, vol.80, pp216, 1996.
- 2.26. L. Pavesi, M. Ceschini, *Phys. Rev. B: Condens. Matter Mater. Phys.*, vol. 48, (17) pp625, 1993.
- 2.27. E. Martin, C. Delerue, G. Allan, M. Lannoo, *Phys. Rev. B: Condens. Matter Mater. Phys.*, vol.50, (18) pp258, 1994.
- 2.28. H. E. Roman, L. Pavesi, *J. Phys.: Condens. Matter*, vol.8, pp5161, 1996.

## Chapter 2

### *Erbium Doped Materials*

---

- 2.29. ST Microelectronics. <http://eu.st.com>, 2002.
- 2.30. Johannes Heitmann, Frank Muller, Margit Zacharias, and Ulrich Gosele, Silicon Nanocrystals: Size Matters, *Adv. Mater.*, vol.17, No. 7, 2005.

**CHAPTER - 3**

**ERBIUM DOPED  
TANTALUM  
PENTOXIDE**

### **3.1. Introduction**

Tantalum pentoxide ( $Ta_2O_5$ ) is well known because of its interesting optical and electrical properties. It has been extensively studied both experimentally and theoretically over the past four decades. Historically,  $Ta_2O_5$  emerged in the seventies, mainly due to its promising properties as an antireflective coating for optical and photovoltaic applications. During the following decade, a few studies explored different ways to obtain stable oxide layers and their potential applications. However, the real emergence of tantalum pentoxide as a dielectric material happened during the last decade primarily because of an exceptional effort in the development of electronics devices using tantalum oxide films as dielectric layers. Such an inflation of studies has been further motivated by the dramatic scaling-down of silicon integrated circuits that has pushed conventional dielectric films (silicon dioxide or silicon nitride) close to their physical limit in terms of reduction of thickness and dielectric strength [3.1-3.6]. This has led to the study of insulators with high dielectric permittivity, such as  $TiO_2$ ,  $Y_2O_3$ ,  $(Ba,Sr)TiO_3$ ,  $Pb(Zr,Ti)O_3$  and  $Ta_2O_5$  which enable an increase of the packing density of devices without a further reduction of insulator thickness [3.7-3.14]. Among these dielectrics, tantalum pentoxide, having a high dielectric constant (depending upon deposition conditions), appears to have been adopted for this purpose because it can be readily deposited using conventional methods which are compatible with equipment already available in process lines (in particular for dynamic random access memory (DRAM) applications at the present time).

The increase in the DRAM density up to 1 Gbit creates a serious problem to ensure the required storage capacitance in trench three-dimensional (3-D) stacked-capacitor cell and technologies based on the  $SiO_2/Si_3N_4/SiO_2$  (ONO) stacked capacitor. To satisfy DRAM requirements of 1 Gbit and beyond higher dielectric constant materials

are necessary to keep the capacitor cells structures simple and easy to fabricate [3.15-3.17]. Among those new dielectrics, Ta<sub>2</sub>O<sub>5</sub> has received considerable attention, because of its high dielectric constant (~35), high refractive index and chemical and thermal stability with the promise of compatibility with microelectronics processing [3.18].

In the last few years, optical properties of Ta<sub>2</sub>O<sub>5</sub> and rare-earth-doped tantalum oxide films have been studied and researched extensively. Interesting optical properties also have been reported from Ta<sub>2</sub>O<sub>5</sub> beyond these electronic properties. Recently Miura et al. have reported blue light emission from RF-sputtered thin films [3.19]. Zhu et al. reported red light emission from amorphous tantalum pentoxide films [3.20]. Also tantalum pentoxide is transparent in the near UV spectral region ( $\lambda > 300$  nm), which is an important point for optoelectronic devices that operate in the ultraviolet, such as terrestrial-based astronomical charge-coupled device (CCD) imagers and space-based photovoltaic devices. In this dissertation we also observed green light emission from TaO<sub>x</sub> thin films.

### **3.2. Fabrication of Ta<sub>2</sub>O<sub>5</sub> thin films with various deposition techniques**

Successful applications of any thin film material require the development of sophisticated synthesis and processing techniques, the understanding of structure property relationships and the implementation of various novel devices.

Thin film deposition is one of the key processes used in optoelectronics and microelectronics manufacturing to fabricate high quality layers for dielectric applications, photonics application, and contact or protective films. Over the past decades, various deposition methods for tantalum pentoxide thin films have been proposed, researched and evaluated. Each deposition method has its advantages and

## Chapter 3

### *Erbium Doped Tantalum Pentoxide*

---

disadvantages related to the deposition mechanisms and film properties. Various efforts have been made to enhance the quality of tantalum pentoxide thin films to make it suitable for advanced optical and dielectric applications.

**Ta<sub>2</sub>O<sub>5</sub> films can be fabricated by different techniques such as –**

- Anodic or thermal oxidation of tantalum layers [3.21-3.31],
- Sputtering [3.32-3.49],
- Vacuum evaporation [3.50-3.54],
- Atomic layer deposition (ALD), also referred as atomic layer epitaxy (ALE) [3.55-3.59],
- Ion-assisted deposition (IAD) [3.60-3.65]
- Sol-gel methods [3.66-3.70].

The most commonly used processes are those based on chemical vapor deposition (CVD) [3.71-3.77], which can currently be considered as a standard method in silicon-based integrated circuit technology.

We will limit our discussion here on three frequently used deposition techniques CVD, sol-gel and sputtering.

#### **3.2.1. Chemical vapor deposition (CVD)**

Chemical vapor deposition is now a standard method in silicon-based integrated technology for the production of thin films (especially low-pressure chemical vapor deposition (LPCVD) and plasma-enhanced chemical vapor deposition (PECVD)).

### Chapter 3

#### *Erbium Doped Tantalum Pentoxide*

---

CVD is generally preferred for insulator manufacture, whereas physical vapor deposition (PVD) is preferentially used for the fabrication of metallic contacts (evaporation or sputtering techniques). In the CVD process, the gaseous reactants (or the vapors obtained from liquid or solid reagents), diluted in an inert gas (hydrogen, helium, argon, etc.) flow over the substrate maintained at relatively high temperature. Carrier gas serves to reduce the concentration of each reactive gas so that they can be safely mixed without spontaneous reactions. These gases also provide sufficient volume to the mixture to force it over the heated substrate, a condition necessary for film deposition. Finally, it allows optimization of gas convection and turbulence conditions necessary to establish good film uniformity. The main advantage of this technique is that it can be performed over a wide pressure range from atmospheric to ultra high vacuum. Moreover, uniform, conformal and adherent layers may be formed.

For example, for thickness and step coverage, chemical vapor deposition of Ta<sub>2</sub>O<sub>5</sub> appears to be superior to reactive sputtering for applications such as the three-dimensional memory capacitors. Furthermore, one can obtain faster deposition rates, reduction of the cost per wafer and better outputs in mass production using CVD [3.78-3.79]. The disadvantages of this method are the manipulation of toxic, explosive or corrosive gases in many processes and the use of comparatively high temperatures (in the range 400-1100°C). Several chemical vapor deposition methods have been employed to produce Ta<sub>2</sub>O<sub>5</sub> thin films as:

- Atmospheric pressure CVD [3.71-3.73],
- Low pressure CVD [3.79-3.87],
- Plasma-enhanced CVD [3.88-3.94],
- Photo-assisted CVD [3.95-3.96],
- Excimer laser assisted CVD [3.97-3.103],
- LPCVD and PECVD are the most frequently employed.



### **3.2.2. Sputtering**

Tantalum pentoxide thin films can be fabricated by sputtering from a tantalum or tantalum oxide target at low pressure in the presence of an oxygen atmosphere with or without an inert gas (the most commonly employed gas is argon) [3.33-3.49]. Deposition of tantalum pentoxide on silicon substrates has been achieved in two ways:

- By direct sputtering when the target is tantalum pentoxide and
- By reactive sputtering when tantalum metal is sputtered in an oxygen ambient.

The deposition rate depends mainly on the RF power and on the different gas pressures. This method has many advantages as it can be performed at relatively low temperatures (in the range 150°-400°C), this method is suitable for mass production as single target is required and films are relatively less contaminated. The main challenge in this technique is: the film stoichiometry is rather difficult to control. If it can be suitably controlled, sputtering may potentially offer considerable material flexibility. Sputtered Ta<sub>2</sub>O<sub>5</sub> films presents similar characteristics to those of deposited by CVD. The principle of RF-sputtering method, experimental setup of sputtering system, and processing conditions has been discussed in detail in chapter 4.

### **3.2.3. Sol-gel method**

The fabrication of thin films by sol-gel method has recently received increased attention. A number of oxides can be deposited, such as oxides of Ti, Zr, Hf, Ta and Si. Sol-gel technique has many advantages, such as low temperature processing, simple and compact equipment, deposition on a substrate characterized by a large area and a complex structure, and high homogeneity of the deposited films. However, the

layers are generally porous and contain large amounts of CH-based species, which can be removed by thermal treatments. The refractive index of the film can also be controlled within limits by the specific method used during layer formation. Controlling this protocol allows the formation of transparent and pinhole-free layers, instead of opaque films with or without pinholes and cracks. This control allows the sol-gel method to produce a wide variety of thin film materials, ranging from dense dielectric films for electronic applications to antireflective coatings for optical applications. Uniform films with different compositions can also be fabricated.

### **3.3. Properties of tantalum pentoxide thin films**

In this section we will review the main characteristics and properties of tantalum pentoxide thin films depending on the preparation method:

- Physical and optical properties (density, refractive index, optical loss, optical band gap),
- Structural properties,
- Chemical properties (etching and resistance to corrosion), electrical properties (dielectric constant, breakdown strength, trapping phenomena, leakage current densities, conduction mechanisms of thin layers)
- Radiation effects on the electrical properties.

#### **3.3.1. Physical and optical properties**

Physical and optical properties of tantalum pentoxide thin films were intensively investigated with respect to their potential applications in solid-state devices, and optical devices.

### Chapter 3

#### *Erbium Doped Tantalum Pentoxide*

---

Table-3.1 presents the values of the density, refractive index and optical loss of tantalum oxide obtained by various techniques.

**Table-3.1. Physical and optical properties of Ta<sub>2</sub>O<sub>5</sub> thin films for different sample preparation techniques**

Sample Preparation	Density (g cm <sup>-3</sup> )	Refractive Index	Optical Loss (dB cm <sup>-1</sup> )	References
Thermal Oxidation		2.28 at 488.0 nm 2.25 at 514.5 nm 2.21 at 632.8 nm	4.1 at 488.0 nm 0.9 at 632.8 nm	[3.110]
Sputtering			1 at 632.8 nm	[3.37]
ALE		1.9 to 2.25		[3.59]
IAD	6.1 to 7.5	1.93 to 2.15 at 633 nm		[3.64]
ECR PECVD		2.12 to 2.16 at 632.8 nm		[3.111]
UV-photo-CVD		2.2 at 546.1 nm		[3.112]

#### **3.3.2. Structural properties of the crystalline phase**

Crystalline tantalum pentoxide presents in two phases:

- **Orthorhombic phase and**
- **Hexagonal phase**

### Chapter 3

#### *Erbium Doped Tantalum Pentoxide*

---

The orthorhombic structure can be divided into two forms, with a reversible transition occurring at about 1360°C:

- A high-temperature form [3.104-3.105] and
- A low-temperature form called L-Ta<sub>2</sub>O<sub>5</sub> [3.106-3.107].

The lattice parameters for orthorhombic-Ta<sub>2</sub>O<sub>5</sub> are  $a = 6.198 \text{ \AA}$ ,  $b = 40.290 \text{ \AA}$  and  $c = 3.888 \text{ \AA}$ . Stephenson and Roth [3.107] studied the structure of the low-temperature form of orthorhombic-Ta<sub>2</sub>O<sub>5</sub>. The orthogonal unit cell of this compound contains 11 formula units. The structure was solved in projection from the Patterson functions. The ideal structure for L-Ta<sub>2</sub>O<sub>5</sub> can be generated from a chain of 8-edge-sharing pentagons. The plane group of the (001) projection of this ideal structure is *pgm*, and the ideal unit cell contains 22 Ta atoms and 58 O atoms. The real structure contains on the average three distortion planes per unit cell, so that one has a reduction in the coordination number of some metal atoms: the real unit cell of L-Ta<sub>2</sub>O<sub>5</sub> contains 22 Ta atoms and 55 O atoms. The distortion planes are statistically distributed over four sites; thereby giving the average unit cell a higher symmetry than the real unit cell.

For the hexagonal phase, the lattice parameters are  $a = 3.62 \text{ \AA}$  and  $c = 3.87 \text{ \AA}$ . Fukumoto and Miwa [3.109] used first-principle calculations to predict the crystal structure of hexagonal Ta<sub>2</sub>O<sub>5</sub> since it is still unknown. Three crystal structures were chosen for evaluation, after referring to the XRD data: *P6/mmm*, *P6m2* and *P63/mmc*.

Their results show that the predicted structure has the space group of *P6/mmm* with two formula units in the unit cell ( $a = 7.191 \text{ \AA}$  and  $c = 3.831 \text{ \AA}$ ;  $a$  is assumed to be twice as large as the measured value due to the extinction rule), and that the coordination number of O atoms to Ta atoms is 8 for one Ta atom and 6 for the other three Ta atoms.

### **3.4. Er-Doped tantalum pentoxide films**

Er-doped materials have attracted great attention due to their usability in optical fiber communication and integrated photonics. The development of integrated optical amplifiers operating in the 1.55 $\mu\text{m}$  band, based on glassy planar waveguides activated by  $\text{Er}^{3+}$  ions, is now a hot research topic. Silica-based matrices are very attractive because of the good solubility of rare-earth ions ( $\sim 6 \times 10^{-20} \text{ cm}^3$ ), of their high optical quality, and chemical robustness. Various fabrication techniques have been employed to fabricate silica based Er-doped waveguides as sol-gel, sputtering, and ion-implantation. Sputtered and sol-gel waveguides seem more suitable for optical amplifiers to be used in WDM systems, due to their wide bandwidth, while ion-exchanged ones may be more convenient for integrated optical lasers.

Erbium-doped fiber amplifiers are commercially available but erbium-doped waveguide amplifiers efficiency can not be compared with EDFAs due to low absorption cross section of erbium and low solubility of  $\text{Er}^{3+}$  in silica matrices.

To overcome these two problems many solutions have been proposed. To increase the efficiency of  $\text{Er}^{3+}$ , it is proposed to co-doping with other rare earth-ions as Yb. Yb has larger absorption area and can transfer its energy to Er.

Tantalum pentoxide can be a possible solution for low solubility of Er in  $\text{SiO}_2$  host material.  $\text{TaO}_x$  is superior to  $\text{SiO}_2$  and  $\text{GeO}_2$  in terms of both the phonon energy and  $\text{Er}^{3+}$  solubility. Amorphous  $\text{Ta}_2\text{O}_5$  has better  $\text{Er}^{3+}$  solubility than  $\text{SiO}_2$  because of the relatively large amount of edge oxygen having a negative charge [3.108].

We fabricated Er-doped thin films with tantalum pentoxide as host material and observed green light emission. We are presenting these results in this dissertation.

## **Chapter 3**

### ***Erbium Doped Tantalum Pentoxide***

---

Details of thin films fabrication and light emission properties can be found in the next chapters. Such thin films can be possibly used in optical amplification devices in integrated optics and light emitting devices.

#### **3.5. Summary**

Ta<sub>2</sub>O<sub>5</sub> and Er-doped Ta<sub>2</sub>O<sub>5</sub> films can be fabricated with various deposition methods. Physical and optical properties of these materials also depend upon the deposition techniques used for film fabrication. Sputtering method can be useful for mass production of thin films. Such deposited films can be used in different photonic devices.

**WORKS CITED**

- 3.1. C. Fiegna, H. Iwai, T. Wada, M. Saito, E. Sangiorgi, B. Ricco, IEEE Trans. Electron Devices ED-41, pp941, 1994.
- 3.2. S. Lai, Semiconductor Silicon 1981, in: H.R. Huff, R.J. Kriegler, Y. Takeishi (Eds.), The Electrochemical Society, Pennington, 1981, p. 4t6.
- 3.3. S. Asai, IEDM Tech. Dig. 6, 1984.
- 3.4. C. Hu, IEDM Tech. Dig. 368, 1985
- 3.5. J. Yugami, T. Mine, S. Iijima, A. Hiraiwa, Ext. Abs. of the 1989 Int. Conf. on Solid State Devices and Materials, Tokyo, Japan, Aug. 23, pp173, 1989.
- 3.6. T. Morimoto, H.S. Momose, M. Tsuchiaki, Y. Ozawa, K. Yamabe, H. Iwai, Ext. Abs. of the 1991 Int. Conf. on Solid State Devices and Materials, Yokohama, Japan, Aug.25, Tokyo, pp.23, 1991.
- 3.7. N. Rausch, E.P. Burte, Microelectron. Eng. 19, pp725, 1992.
- 3.8. S.A. Campbell, D.C. Gilmer, X.C. Wang, M.T. Hsieh, H.S. Kim, W.L. Gladfelter, J. Yah, IEEE Trans. Electron Devices ED-44, pp104, 1997.
- 3.9. M. Gurvitch, Appl. Phys. Lett. 51,1987.
- 3.10. R. Khamankar, J. Kim, B. Jiang, C. Sudhama, P. Maniar, R. Moazzami, R. Jones, J. Lee, IEDM Tech. Dig. 337, 1994.
- 3.11. Y.M. Corc, O. Musseau, J.L. Leray, IEEE Trans. Nucl. Sci. NS-41, pp495, 1994.
- 3.12. J.L. Autran, P. Paillet, J.L. Leray, R.A.B. Devine, Le Vide: Science, Technique et Applications 275, 44, 1995.
- 3.13. Y.S. Choi, S.D. Choe, S.H. Kim, C.E. Kim, D.Y. Yang, Mater. Res. Soc. Symp. Proc. 446, pp337, 1997.

### Chapter 3

#### *Erbium Doped Tantalum Pentoxide*

---

- 3.14. T. Li, P. Zawadzki, R.A. Stall, Y. Zhu, S.B. Desu, Mater. Res. Soc. Symp. Proc. 446, pp315, 1997.
- 3.15. M. Koyanagi, H. Sunami, N. Hashimoto, and M. Ashikawa, IEDM Tech. Dig. 348,1978.
- 3.16. H. Sunami, T. Kure, N. Hashimoto, K. Itoh, T. Toyabe and S. Asai , IEEE Trans. Electron Devices 31, 746,1984.
- 3.17. K. Minegishi, S. Nakajima, K. Miura , K . HARADA and T. Shibata, IEDM Tech. Dig. 319, pp33, 1983.
- 3.18. S. Ezhilvalavan, T. Y. Tseng, Preparation and properties of tantalum pentoxide ( $Ta_2O_5$ ) thin films for ultra large scale integrated circuits (ULSIs) application- A review, Journal of materials science: Materials in electronics 109-31, 1999.
- 3.19. K. Miura, H. Miyazaki, and O. Hanaizumi, "Observation of blue-light emission from tantalum oxide films deposited by using radio-frequency magnetron sputtering," IEICE Trans. Electron., vol. E91-C, no. 10, pp. 1669–1672, 2008.
- 3.20. M. Zhu, Z. Zhang, and W. Miao, "Intense photoluminescence from amorphous tantalum oxide films," Appl. Phys. Lett., vol. 89, no.2, pp. 021915–021915–3, 2006.
- 3.21. L. Young, Proc. R. Soc. London A 244, pp4I, 1958.
- 3.22. L. Young, Proc. R. Soc. London A 258, pp496, 1960.
- 3.23. C.L. Standley, L.I. Maissel, J. Appl. Phys. 35, pp1530, 1964.
- 3.24. D. Gerstenberg, J. Electrochem. Soc. 113, pp542, 1966.
- 3.25. D. Mills, L. Young, F.G.R. ZobeI, J. Appl. Phys. 37, pp1821, 1966.
- 3.26. N.N. Axelrod, N. Schwartz, J. Electrochem. Soc. 116, pp460, 1969.



### Chapter 3

#### *Erbium Doped Tantalum Pentoxide*

---

- 3.27. C.J. Dell'Oca, Y. Young, J. Electrochem. Soc. 117, pp1548, 1970.
- 3.28. G.D. O'Clock Jr., Appl. Phys. Lett. 19, pp403, 1971.
- 3.29. P.S. Wilcox, W.D. Westwood, Can. J. Phys. 49, pp1543, 1971.
- 3.30. J.P.S. Pringle, J. Electrochem. Soc. 119, pp482, 1972.
- 3.31. J.P.S. Pringle, J. Electrochem. Soc. i20, pp398, 1973.
- 3.32. F. Vratny, J. Electrochem. Soc. 114, pp505, 1967.
- 3.33. W.D. Westwood, R.J. Boynton, S.J. Ingre, J. Vac. Sci. Technol. 1i, pp381, 1974.
- 3.34. D.M. Hughes, M.W. Jones, J. Phys. D 7, pp208I, 1974.
- 3.35. E.E. Khawaja, S.G. Tomlin, Thin Solid Films 30, pp361, 1975.
- 3.36. L.G. Meiners, R.P. Pan, J.R. Sites, J. Vac. Sci. Technol. 14, pp961, 1977.
- 3.37. W.M. Paulson, F.S. Hickernell, R.L. Davis, J. Vac. Sci. Technol. 16 (1979) 307.
- 3.38. F. Rubio, J.M. Albella, J. Denis, J.M. Martinez-Duart, J. Vac. Sci. Technol. 21 (1982) 1043.
- 3.39. T.M. Reith, P.J. Ficarola, J. Vac. Sci. Technol. A 1 (1983) 1362.
- 3.40. S. Seki, T. Unagami, B. Tsujiyama, J. Vac. Sci. Technol. A i (1983) 1825.
- 3.41. S. Kimura, Y. Nishioka, A. Shintani, K. Mukai, J. Electrochem. Soc. 130 (1983) 2414.
- 3.42. S. Seki, T. Unagami, O. Kogure, J. Electrochem. Soc. 132 (1985) 3054.
- 3.43. H. Demiryont, J.R. Sites, K. Geib, Appl. Opt. 24 (1985) 490.
- 3.44. S. Roberts, J. Ryan, L. Nesbit, J. Electrochem. Soc. 133 (1986) I405.

### Chapter 3

#### *Erbium Doped Tantalum Pentoxide*

---

- 3.45. S. Seki, T. Unagami, O. Kogure, B. Tsujiyama, *J. Vac. Sci. Technol. A* 5 (1987) 1771.
- 3.46. Y. Nishioka, S. Kimura, H. Shinriki, K. Mukai, *J. Electrochem. Soc.* 134 (1987) 410.
- 3.47. U. Teravaninthorn, Y. Miyahara, T. Moriizumi, *Jpn. J. Appl. Phys.* 26 (1987) 347.
- 3.48. T. Kato, T. Ito, *J. Electrochem. Soc.* 135 (1988) 2586.
- 3.49. Y.K. Tu, C.C. Lin, W.S. Wang, S.L. Huang, *Thin Solid Films* 162 (1988) 325.
- 3.50. J.G. Hwu, M.J. Jeng, W.S. Wang, Y.K. Tu, *J. Appl. Phys.* 62 (1987) 4277.
- 3.51. H.O. Sankur, W. Gunnig, *Appl. Opt.* 28 (1989) 2806.
- 3.52. F. Gitmans, Z. Sitar, P. Gtinter, *Vacuum* 46 (1995) 939.
- 3.53. J. Hudner, P.E. Hellberg, D. Kusche, H. Ohls6n, *Thin Solid Films* 281-282 (1996) 415.
- 3.54. J.V. Grahn, P.E. Hellberg, E. Olsson, *J. Appl. Phys.*, (in press).
- 3.55. M. Pessa, R. Makela, T. Suntola, *Appl. Phys. Lett.* 38 (1981) 131.
- 3.56. H. Kattelus, M. Ylilamini, J. Saarrilahti, J. Antson, S. Lindfors, *Thin Solid Films* 225 (1993) 296.
- 3.57. H. Kattelus, M. Ylilammi, J. Salmi, T. Ranta-Aho, E. Nyk~inen, I. Suni, *Mater. Res. Sec. Symp. Proc.* 284 (1993) 511.
- 3.58. J. Aarik, A. Aidla, K. Kukli, T. Uustare, *J. Cryst. Growth* 144 (1994) t 16.
- 3.59. K. Kukli, M. Ritala, M. Lesket~i, *J. Electrochem. Soc.* 142 (1995) 1670.
- 3.60. H. Siimon, J. Aarik, *J. Phys. IV* 5 (1995) C5-277.
- 3.61. K. Kukli, J. Am'ik, A. Aidla, O. Kohan, T. Uustare, V. Sammetselg, *Thin Solid Films* 260 (1995) 135.

### Chapter 3

#### *Erbium Doped Tantalum Pentoxide*

---

- 3.62. J.J. McNally, G.A. Al-Jumaily, J.R. McNeil, *J. Vac. Sci. Technol. A* 4 (1986) 437.
- 3.63. P.J. Martin, A. Bendavid, M. Swain, R.P. Netterfield, T.J. Kinder, W.G. Sainty, D. Drage, L. Wielunski, *Thin Solid Films* 239 (1994) 181.
- 3.64. P.M. Natishan, E. McCafferty, P.R. Puckett, S. Michel, *Corros. Sci.* 38 (1996) 1043.
- 3.65. Q. Tang, S. Ogura, K. Kikuchi, N. Higashi, *Rev. Laser Eng.* 24 (1996) 110.
- 3.66. T.J. Rehg, J.A. Ochoa-Tapia, A. Knoesen, B.G. Higgins, *Appl. Opt.* 28 (1989) 5215.
- 3.67. M.M. Blouke, M.D. Nelson, M. Serra, A. Knoesen, B.G. Higgins, W.A. Delamere, G. Womack, J.S. Flores, M. Duncan, R. Reed, *Proc.* 1656 (1992) 497.
- 3.68. T. Oishi, T. Nakazawa, A. Katou, *Electron. Com. Jpn.* 76 (1993) 50.
- 3.69. T. Ohishi, A. Katoh, *Br. Ceram. Trans.* 92 (1993) 79.
- 3.70. N. Ozer, C.M. Lampert, *J. Sol-Gel Sci. Technol.* 8 (1997) 703.
- 3.71. T. Takahashi, H. Itoh, *J. Less-Common Met.* 38 (1972) 2tl.
- 3.72. W.H. Knausenberger, R.N. Tauber, *J. Electrochem. Soc.* 120 (1973) 927.
- 3.73. E. Kaplan, M. Balog, D. Frohman-Bentchkowsky, *J. Electrochem. Soc.* 123 (1976) 1570.
- 3.74. S. Zaima, T. Furuta, Y. Yasuda, M. Tida, *J. Electrochem. Soc.* 137 (1990) I297.
- 3.75. E.P. Butte, N. Rausch, in: W. Eccleston, M. Urer (Eds.), *Proc. of the 7th Biennial European Conf. on Insulating Films on Semiconductors*, Liverpool, England, April 2-5, 1991, Adam Hilger, Bristol, 1991, p. 199.
- 3.76. H. Shinriki, M. Nakata, *IEEE Trans. Electron Devices* ED-38 (1991) 455
- 3.77. W. Kern, R.S. Rosler, *J. Vac. Sci. Technol.* 14 (1977) 1082.

### Chapter 3

#### *Erbium Doped Tantalum Pentoxide*

---

- 3.78. A.C. Adams, C.D. Capio, J. Electrochem. Soc. 126 (1979) 1042.
- 3.79. K. Tominaga, R. Muhammet, I. Kobayashi, M. Okada, Jpn. J. Appl. Phys. 31 (1992) L585.
- 3.80. G.Q. Lo, D.L. Kwong, S. Lee, Appl. Phys. Lett. 60 (1992) 3286.
- 3.81. H. Treichel, A. Mitwalsky, N.P. Sandler, D. Tribula, W. Kern, A.P. Lane, Adv. Mater. Opt. Electron. 1 (1992) 299.
- 3.82. S. Kamiyama, P.Y. Lesaicherre, H. Suzuki, A. Sakai, I. Nishiyama, A. Ishitani, J. Electrochem. Soc. 140 (1993) 1617.
- 3.83. K.W. Kwon, C.S. Kang, T.S. Park, Y.B. Sun, N. Sandler, D. Tribula, Mater. Res. Soc. Symp. Proc. 284 (1993) 505.
- 3.84. C.H. An, K. Sugimoto, J. Electrochem. Soc. 139 (1994) 853.
- 3.85. S.C. Sun, T.F. Chen, IEDM Tech. Dig. (1994) 333.
- 3.86. S. Kamiyama, H. Suzuki, P.Y. Lesaicherre, A. Ishitani, IEICE Trans. Electron. E77-C (1994) 379.
- 3.87. Y. Matsui, K. Torii, M. Hirayama, Y. Fujisaki, S. Iijima, Y. Ohji, IEEE Electron Device Lett. EDL-17 (1996) 431.
- 3.88. S.O. Kim, J.O. Byun, H.J. Kim, Thin Solid Films 206 (1991) I02.
- 3.89. H.S. Pro'k, Y. K. Baek, J.C. Kim, S.H. Choi, K.H. Oh, Ext. Abs. of the 1992 Int. Conf. on Solid State Devices and Materials, Tsukuba, Japan, August 26-28, 1992, Business Center for Academic Societies Japan, Tokyo, 1992, p. 524.
- 3.90. P.A. Murawala, M. Sawai, T. Tatsuta, O. Tsuji, S. Fujita, S. Fujita, Jpn. J. Appl. Phys. 32 (1993) 368.
- 3.91. Kim, S.D. Ahn, B.W. Cho, S.T. Ahn, J.Y. Lee, J.S. Chun, W.J. Lee, Jpn. J. Appl. Phys. 33 (1994) 6691.
- 3.92. D. Laviale, J.C. Oberlin, R.A.B. Devine, Appl. Phys. Lett. 65 (1994) 2021.

### Chapter 3

#### *Erbium Doped Tantalum Pentoxide*

---

- 3.93. H.S. Moon, J.S. Lee, S.W. Han, J.W. Park, J.H. Lee, S.K. Yang, H.H. Park, J. Mater. Sci. 29 (1994) 3372.
- 3.94. S.K. Jeon, S.W. Han, J.W. Park, J. Appl. Phys. 77 (1995) 5978.
- 3.95. K. Yamagishi, Y. Tarui, Jpn. J. Appl. Phys. 25 (1986) L306.
- 3.96. S. Tanimoto, M. Matsui, M. Aoyagi, K. Kamisako, K. Kuroiwa, Y. Tarui, Jpn. J. Appl. Phys. 30 (1991) L330.
- 3.97. Y. Imai, A. Watanabe, K. Osato, T. Kameyama, K. Fukuda, Chem. Lett. (1990) 177.
- 3.98. Y. Nishimura, K. Tokunaga, M. Tsuji, Thin Solid Films 226 (1993) 144.
- 3.99. M. Mukaida, K. Osato, A. Watanabe, Y. Imai, T. Kameyama, K. Fukuda, Thin Solid Films 232 (1993) 180.
- 3.100. A. Watanabe, M. Mukaida, Y. Imai, K. Osato, T. Kameyama, K. Fukuda, J. Mater. Sci. 28 (1993) 5363.
- 3.101. Y. Imai, A. Watanabe, M. Mukaida, K. Osato, T. Tsunoda, T. Kameyama, K. Fukuda, Thin Solid Films 261 (1995) 76.
- 3.102. A. Watanabe, M. Mukaida, K. Osato, Y. Imai, T. Kameyama, K. Fukuda, J. Mater. Sci. 30 (1995) 4603.
- 3.103. N. Inoue, S. Kashiwabara, S. Toshima, R. Fujimoto, Appl. Surf. Sci. 96-98 (1996) 656.
- 3.104. S. Lagergren, A. Magneli, Acta Chem. Scand. 6 (1952) 444.
- 3.105. F. Laves, W. Petter, Helv. Phys. Acta 12 (1964) 617.
- 3.106. R. Moser, Schweiz. Mineral. Petrogr. Mitt. 45 (1965) 35.
- 3.107. N.C. Stephenson, R.S. Roth, Acta Crystatlogr. Sect. B 27 (1971) 1037.
- 3.108. R. J. Cava, W. F. Peck Jr. and J. J. Krajewski, Nature 377 (1995) 215

### Chapter 3

#### *Erbium Doped Tantalum Pentoxide*

---

- 3.109. A. Fukumoto, K. Miwa, Phys. Rev. B 55 (1997) 11155.
- 3.110. D.H. Hensler, J.D. Cuthbert, R.J. Martin, P.K. Tien, Appl. Opt. 10 (1971) 1037.
- 3.111. R.A.B. Devine, L. Vallier, J.L. Autran, P. Paillet, J.L. Leray, Appl. Phys. Lett. 68 (1996) 1775.
- 3.112. S. Tanimoto, Y. Shichi, K. Kuroiwa, Y. Tarui, Ext. Abs. of the 1993 Int. Conf. on Solid State Devices and Materials, Chiba, Japan, August 29-September 1, 1993, Business Center for Academic Societies Japan, Tokyo, 1993, p. 859.

**CHAPTER - 4**

**EXPERIMENTAL  
DESIGN**

#### **4.1. Introduction**

Thin-film growth techniques have fundamentally changed both condensed matter physics and everyday life. Well established thin-film technologies are used to grow the integrated circuits in computers, cell phones, and many other electronics and optoelectronics devices. Many of the techniques used to grow thin films are related, and involve physics and technology of marvelous subtlety. In this chapter, we discuss the design, fabrication, and characterization of the thin films studied throughout this thesis.

#### **4.2. Different fabrication techniques**

Various thin film deposition techniques are used for different requirements, such as-

- Thermal evaporation,
- Pulsed laser deposition,
- Radio-frequency (RF) sputtering,
- Low-Pressure CVD (LPCVD),
- Plasma-Enhanced CVD (PECVD),
- Metal-Organic CVD (MOCVD) etc.

We selected RF-sputtering for thin film fabrication in our samples. Sputtering method has some advantages over the other deposition methods. Sputter deposited films have a composition close to that of the source material. They have a better adhesion on the substrate than the evaporated films. In addition sputtering method is more suitable for mass production as single target is required for sputtering and film are relatively less contaminated.



### 4.3. RF-sputtering

Sputtering is a vacuum evaporation process, which physically removes portions of a coating material called the target, and deposits a thin, firmly bonded film onto an adjacent surface called the substrate. Sputtering has proven to be a successful method of coating a variety of substrates with thin films of electrically conductive or non-conductive materials. One of the most striking characteristics of sputtering is its universality. Since the coating material is passed into the vapor phase by a mechanical rather than a chemical or thermal process, virtually any material can be deposited. During sputtering process direct current is used to sputter conductive materials, while radio frequency is used for non-conductive materials. Before starting the sputtering process a vacuum of  $0.5 \times 10^{-4}$  to  $1.0 \times 10^{-4}$  Pa must be achieved. From this point a closely controlled flow of an inert gas such as argon is introduced. This raises the pressure to the minimum needed to operate the magnetrons, although it is still only a few ten thousandth of atmospheric pressure. During the sputter process a magnetic field can be used to trap secondary electrons close to the target. The electrons follow helical paths around the magnetic field lines undergoing more ionizing collisions with neutral gaseous near the target. This enhances the ionization of the plasma near the target leading to a higher sputter rate. It also means that the plasma can be sustained at a lower pressure. The sputtered atoms are neutrally charged and so are unaffected by the magnetic trap. There are various applications of great importance include thin films:

- Optical waveguide materials - Si, Er-doped Silicon, Tantalum, Silicon nanocrystal
- Magnetic materials for data storage tape - Co-Ni, Tb-Fe and Co-Ni-Cr.
- Optical materials for lens characteristics -  $\text{CeO}_2$ , MgO and  $\text{MgF}_2$ .

- Lubricant materials for reducing friction - MoS<sub>2</sub>, WS<sub>2</sub>.
- Wear-resistant materials to lengthen cutting tool life - TiN, TiC, and ZrB<sub>2</sub>.
- Metalizing materials for microcircuits - Al, W-Ti, Al-Si and Al-Cu.
- Transparent conducting materials - xLn<sub>2</sub>O<sub>3</sub> -ySnO<sub>2</sub>.
- Thin-film resistors - Ni-Cr, Cr-Si and Cr-SiO.
- Amorphous bubble memory devices - Gd-Co. Lu<sub>3</sub>Fe<sub>5</sub>O<sub>12</sub>, and Gd<sub>3</sub>Ga<sub>5</sub>O<sub>12</sub>.

#### **4.4. Experimental details of RF-Sputtering system**

We used RF magnetron sputtering system, (ULVAC, SH-350-SE) to fabricate thin films. The pressure in the vacuum chamber of the sputtering system was  $0.54 \times 10^{-4}$  to  $1.06 \times 10^{-4}$  Pa, the Ar flow rate in the chamber was 10 sccm, and the pressure during deposition was approximately 1.1 Pa. The RF power supplied to the target was 200 to 300 W in different samples. Fused silica plates (thickness 1 mm) were used as substrates. The substrates were not heated during sputtering process. Fig. 4.1 shows the sputtering machine used in film fabrication and Fig. 4.2 shows the schematic diagram of sputtering machine. Fig. 4.3 explains the sputtering process. During sputtering process first Ar ions (blue dots in fig. 4.3) hit the target, this collision ejects particles (yellow dots in fig. 4.3) from the surface. Multiple collisions create a large number of particles ejected from the target. These particles are deposited on substrate and give a uniform layer of desired material.



**Fig. 4.1. Sputtering machine used in film fabrication**

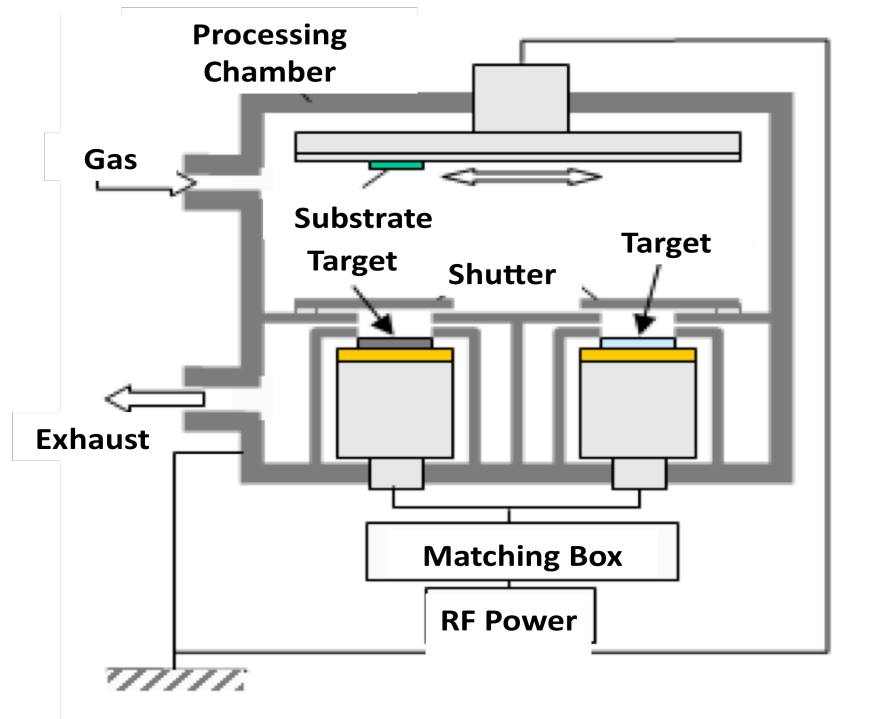


Fig. 4.2. Schematic diagram of sputtering machine

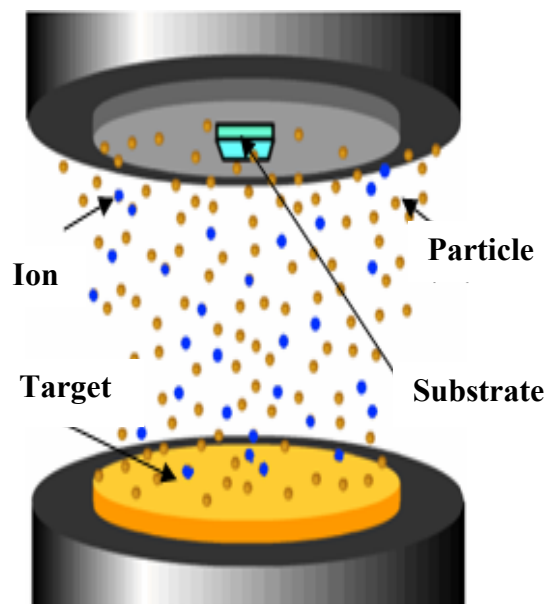


Fig. 4.3. Schematic diagram of sputtering Process

**Fabrication of different thin films**

**Table-4.1. Details of sputtering processing condition for SiO<sub>2</sub> / Er<sub>2</sub>O<sub>3</sub> samples**

<b>Sample (Material)</b>	<b>Vacuum Pressure X 10<sup>-6</sup> Torr</b>	<b>RF Power (W)</b>	<b>Time (min)</b>	<b>Thickness Å</b>	<b>Thickness Å /min</b>	<b>Tablets</b>
SiO <sub>2</sub> /Er <sub>2</sub> O <sub>3</sub>	0.46	200	135	18433	136.5407	Er <sub>2</sub> O <sub>3</sub> × 4
SiO <sub>2</sub> /Er <sub>2</sub> O <sub>3</sub>	0.70	200	183	21867	119.4918	Er <sub>2</sub> O <sub>3</sub> × 4
SiO <sub>2</sub> /Er <sub>2</sub> O <sub>3</sub>	0.69	200	210	24933	118.7286	Er <sub>2</sub> O <sub>3</sub> × 4
SiO <sub>2</sub> /Er <sub>2</sub> O <sub>3</sub>	0.44	200	162	22267	137.4506	Er <sub>2</sub> O <sub>3</sub> × 3
SiO <sub>2</sub> /Er <sub>2</sub> O <sub>3</sub>	0.61	200	145	19800	136.5517	Er <sub>2</sub> O <sub>3</sub> × 2
SiO <sub>2</sub> /Er <sub>2</sub> O <sub>3</sub>	0.59	200	131	19167	146.313	Er <sub>2</sub> O <sub>3</sub> × 1
SiO <sub>2</sub> /Er <sub>2</sub> O <sub>3</sub>	0.55	200	161	11667	72.46584	Er <sub>2</sub> O <sub>3</sub> × 2
SiO <sub>2</sub> /Er <sub>2</sub> O <sub>3</sub>	0.57	200	303	21033	69.41584	Er <sub>2</sub> O <sub>3</sub> × 2
SiO <sub>2</sub> /Er <sub>2</sub> O <sub>3</sub>	0.83	200	161	20433	126.913	Er <sub>2</sub> O <sub>3</sub> × 2
SiO <sub>2</sub> /Er <sub>2</sub> O <sub>3</sub>	0.59	200	267	19350	72.47191	Er <sub>2</sub> O <sub>3</sub> × 2
SiO <sub>2</sub> /Er <sub>2</sub> O <sub>3</sub>	0.64	200	174	20467	117.6264	Er <sub>2</sub> O <sub>3</sub> × 2

We fabricated thin films with different materials and different fabrication condition. We used SiO<sub>2</sub> and Ta<sub>2</sub>O<sub>5</sub> as target materials and put Er<sub>2</sub>O<sub>3</sub> tablets on top of target to fabricate co-doped films.

Er-doped Silicon oxide films were fabricated by RF magnetron sputtering system, [ULVAC, SH-350-SE]. Ta<sub>2</sub>O<sub>5</sub> disc [Furuchi Chemical Corporation, 99.99% purity, diameter- 100 mm] was used as sputtering target. Thin films were deposited by supplying RF power to target. Pressure in vacuum chamber was  $1.6 \times 10^{-4}$ , Ar flow rate in the chamber was 10 sccm and pressure during deposition was around 1.1 Pa. RF power supplied to the SiO<sub>2</sub> target was 300 W, fused silica substrates [ATOCK Inc. 1 mm thickness] were used. Films were annealed from 400°-1000°C in ambient air after fabrication.

Tantalum oxide films were fabricated by RF magnetron sputtering system, [ULVAC, SH-350-SE]. Ta<sub>2</sub>O<sub>5</sub> disc [Furuchi Chemical Corporation, 99.99% purity, diameter- 100 mm] was used as sputtering target. Tantalum oxide films were deposited by supplying RF power to target. Pressure in vacuum chamber was  $1.6 \times 10^{-4}$ , Ar flow rate in the chamber was 10 sccm and pressure during deposition was around 1.1 Pa. RF power supplied to the Ta<sub>2</sub>O<sub>5</sub> target was 300 W, fused silica substrates [ATOCK Inc. 1 mm thickness] were used, and substrates were heated at 250°C. Films were annealed from 400°-1000°C in ambient air after fabrication.

Details of processing conditions for different materials are shown in different tables.

**Table-4.2. Details of sputtering processing condition for Ta<sub>2</sub>O<sub>5</sub> samples**

<b>Sample (Material)</b>	<b>Vacuum Pressure X 10<sup>-6</sup> Torr</b>	<b>Ar Pressure (sccm)</b>	<b>RF Power (W)</b>	<b>Time (min.)</b>	<b>Thickness Å</b>	<b>Thickness Å/min</b>
Ta <sub>2</sub> O <sub>5</sub>	0.46	10	300	60	40200	670
Ta <sub>2</sub> O <sub>5</sub>	0.74	10	300	30	19900	663.33
Ta <sub>2</sub> O <sub>5</sub>	0.75	10	300	120	78300	652.50
Ta <sub>2</sub> O <sub>5</sub>	0.85	10	300	35	19900	663.33
Ta <sub>2</sub> O <sub>5</sub>	0.83	10	300	35	19900	663.33
Ta <sub>2</sub> O <sub>5</sub>	0.53	10	300	35	19900	663.33
Ta <sub>2</sub> O <sub>5</sub>	0.57	10	300	35	19900	663.33
Ta <sub>2</sub> O <sub>5</sub>	0.8	10	200	60	19900	663.33
Ta <sub>2</sub> O <sub>5</sub>	0.78	10	200	60	19900	663.33
Ta <sub>2</sub> O <sub>5</sub>	0.78	15	300	30	19900	663.33
Ta <sub>2</sub> O <sub>5</sub>	0.66	5	300	30	19900	663.33
Ta <sub>2</sub> O <sub>5</sub>	0.64	10	200	60	19900	663.33
Ta <sub>2</sub> O <sub>5</sub>	0.49	10	100	90	19900	663.33
Ta <sub>2</sub> O <sub>5</sub>	0.64	10	300	70	41300	590
Ta <sub>2</sub> O <sub>5</sub>	0.22	10	300	30	19900	663.33
Ta <sub>2</sub> O <sub>5</sub>	0.47	10	300	35	19900	663.33
Ta <sub>2</sub> O <sub>5</sub>	0.41	10	300	35	19900	663.33
Ta <sub>2</sub> O <sub>5</sub>	0.38	10	300	35	21900	625.71
Ta <sub>2</sub> O <sub>5</sub>	0.38	20	300	35	24300	694.29
Ta <sub>2</sub> O <sub>5</sub>	0.67	10	200	35	15200	434.29

**Table 4.3. Details of sputtering processing condition for Ta<sub>2</sub>O<sub>5</sub>/Er<sub>2</sub>O<sub>3</sub> samples**

Sample (Material)	Vacuum Pressure X 10 <sup>-6</sup> Torr	RF Power (W)	Time (min)	Thickness Å	Thickness Å/min	Tablets
Ta <sub>2</sub> O <sub>5</sub> /Er <sub>2</sub> O <sub>3</sub>	0.79	300	35	11200	320	Er <sub>2</sub> O <sub>3</sub> × 3
Ta <sub>2</sub> O <sub>5</sub> /Er <sub>2</sub> O <sub>3</sub>	0.82	300	35	17200	491.4286	Er <sub>2</sub> O <sub>3</sub> × 3
Ta <sub>2</sub> O <sub>5</sub> /Er <sub>2</sub> O <sub>3</sub>	0.73	300	51	25700	503.9216	Er <sub>2</sub> O <sub>3</sub> × 3
Ta <sub>2</sub> O <sub>5</sub> /Er <sub>2</sub> O <sub>3</sub>	0.70	300	50	25667	513.34	Er <sub>2</sub> O <sub>3</sub> × 3
Ta <sub>2</sub> O <sub>5</sub> /Er <sub>2</sub> O <sub>3</sub>	0.77	300	58	26800	462.069	Er <sub>2</sub> O <sub>3</sub> × 3
Ta <sub>2</sub> O <sub>5</sub> /Er <sub>2</sub> O <sub>3</sub>	0.79	300	217	105000	483.871	Er <sub>2</sub> O <sub>3</sub> × 3
Ta <sub>2</sub> O <sub>5</sub> /Er <sub>2</sub> O <sub>3</sub>	0.8	300	35	19433	555.23	Er <sub>2</sub> O <sub>3</sub> × 2
Ta <sub>2</sub> O <sub>5</sub> /Er <sub>2</sub> O <sub>3</sub>	0.79	300	35	16333	466.66	Er <sub>2</sub> O <sub>3</sub> × 3
Ta <sub>2</sub> O <sub>5</sub> /Er <sub>2</sub> O <sub>3</sub>	0.77	300	35	26800	619.06	Er <sub>2</sub> O <sub>3</sub> × 1
Ta <sub>2</sub> O <sub>5</sub> /Er <sub>2</sub> O <sub>3</sub>	0.41	300	35	19600	560.00	Er <sub>2</sub> O <sub>3</sub> × 2



**Table-4.4. Details of sputtering processing condition for Ta<sub>2</sub>O<sub>5</sub> /Er<sub>2</sub>O<sub>3</sub>, Yb<sub>2</sub>O<sub>3</sub> samples**

<b>Sample (Material)</b>	<b>Vacuum Pressure X 10<sup>-6</sup> Torr</b>	<b>RF Power (W)</b>	<b>Sputtering Time (min)</b>	<b>Thickness Å</b>	<b>Thickness Å/min</b>	<b>Tablets</b>
Ta <sub>2</sub> O <sub>5</sub> /Er <sub>2</sub> O <sub>3</sub> , Yb <sub>2</sub> O <sub>3</sub>	0.58	300	35	17433	498.0857	Er <sub>2</sub> O <sub>3</sub> ×2 Yb <sub>2</sub> O <sub>3</sub> ×1
Ta <sub>2</sub> O <sub>5</sub> /Er <sub>2</sub> O <sub>3</sub> , Yb <sub>2</sub> O <sub>3</sub>	0.51	300	35	14367	410.4857	Er <sub>2</sub> O <sub>3</sub> ×2 Yb <sub>2</sub> O <sub>3</sub> ×2
Ta <sub>2</sub> O <sub>5</sub> /Er <sub>2</sub> O <sub>3</sub> , Yb <sub>2</sub> O <sub>3</sub>	0.71	300	35	14300	408.5714	Er <sub>2</sub> O <sub>3</sub> ×3 Yb <sub>2</sub> O <sub>3</sub> ×1
Ta <sub>2</sub> O <sub>5</sub> / Yb <sub>2</sub> O <sub>3</sub>	0.66	300	35	17500	500	Yb <sub>2</sub> O <sub>3</sub> ×2

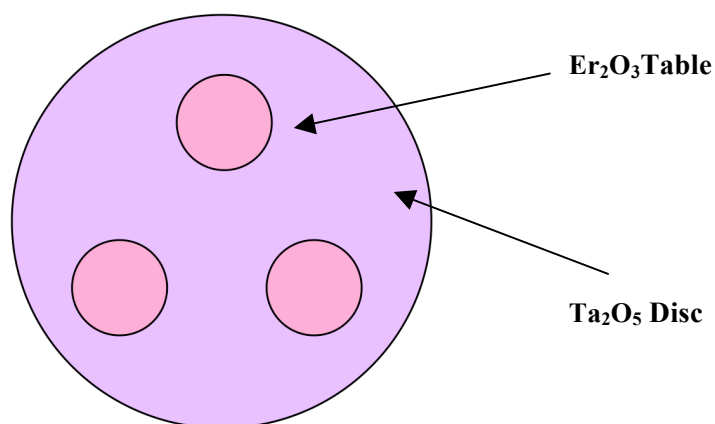


**Fig. 4.4. Target Setup for sputtering**

#### **4.5. Annealing**

Annealing is a heat treatment process that changes physical and optical properties significantly. There are many reported works related to effect of annealing on structural and optical properties of thin films and devices [4.1-4.5].

We used electric furnace (DENKEN Co., Ltd., KDF-S70) for annealing the samples. Fig. 4.5 shows the KDF-S70 electric furnace. Fig.4.6 shows the heating chamber of electric furnace KDF-S70. The samples were placed in the heating chamber of electric furnace DENKEN KDF-S70, which can be heated to a maximum of 1150°C. Typically the samples were heated slowly into a pre-heated state. It takes approximately 40 min to reach the desired temperature. After reaching the desired temperature, chamber's temperature was constant for 20 min. Cooling process takes about 5-6 hours. It is also possible to increase the temperature while the sample is in the furnace. In our experiments we annealed samples in ambient air. We studied various effects of annealing on samples such as, effect of annealing on structural

properties of thin films (e.g. change in film thickness, change in phase and crystal structure), effect of annealing on bandgap of thin films and effect of annealing on light emitting properties of thin films.



**Fig. 4.5. KDF-S70 Electric Furnace**



**Fig. 4.6. Heating chamber of KDF-S70 electric furnace**

#### 4.6. PL Measurement setup

Fig. 4.7 shows the schematic diagram of PL measurement setup. The setup used for the PL measurements is shown in Fig. 4.8. An Helium-cadmium laser (Kimmon, IK3251R-F,) with a wavelength of 325 nm and max power 200 mW was used to excite the samples. The light was collected by a pair of convex lenses, each with focal lengths of 10 cm. One was placed 10 cm away from the sample while the other was placed 10 cm away from the entrance slit of the monochromator so an image of the sample was projected onto the entrance slits. A 325 nm wavelength cut filter was used before entrance slit. We used dual-grating monochromator (Roper Scientific, Spectrapro-2150i, grating size 32 x 32 mm, focal length 150 mm, scan range 0-1400 nm, with  $\pm 0.25$  nm accuracy) and CCD detector (Roper scientific, Pixis-100B, CCD image sensor back-illuminated, 1340 x 100 CCD array 20 x 20- $\mu\text{m}$  pixels) setup to measure PL intensity. We used WinSpec software for automatic data acquisition, analysis and display provided by Princeton instruments.

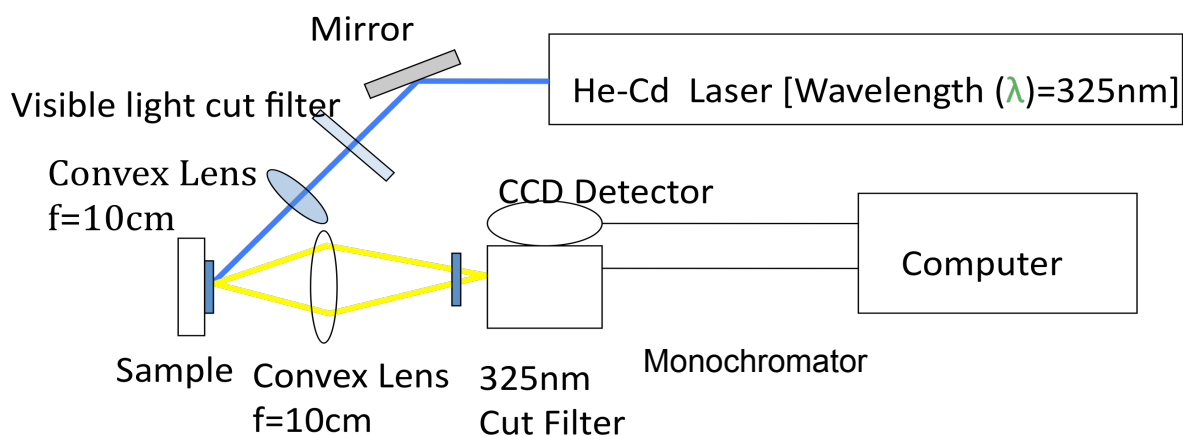


**Fig. 4.7. Schematic diagram of PL measurement setup**

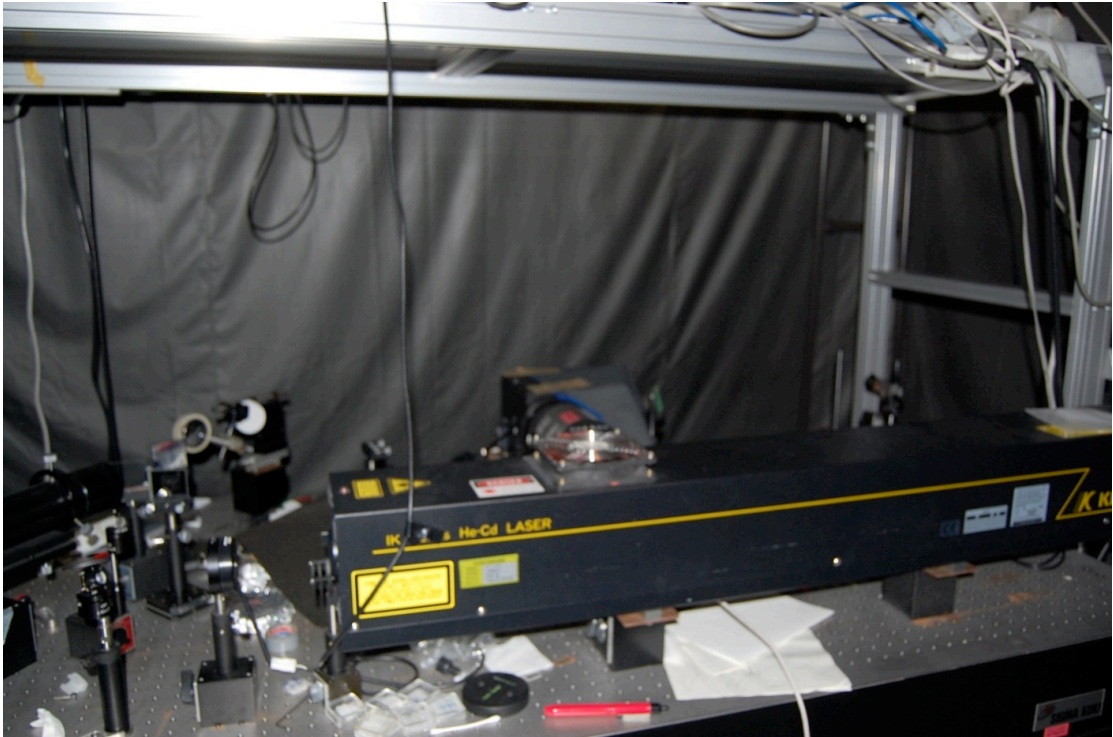


**Fig. 4.8. PL Measurement Setup used in this work**

#### **4.7. Electron Probe Micro Analyzer (EPMA)**

An electron probe micro-analyzer is an instrument used primarily for the non-destructive chemical analysis of minute solid samples. It is same as an scanning electron microscope (SEM) with the added capability of chemical analysis. The primary importance of an EPMA is the ability to acquire precise, quantitative elemental analyses at very small "spot" sizes (as little as 1-2 microns). This instrument has the features that special attention is not necessary in sample handling procedures. The electron optics of an SEM or EPMA allow much higher resolution images to be obtained than can be seen using visible-light optics. We used Shimadzu EPMA-1610 to calculate the concentration of different elements in the samples discussed in this thesis.

#### **Fundamental Principle of Electron Probe Micro Analyzer (EPMA)**

A beam of electrons is fired at a sample. The beam causes each element in the sample to emit X-rays at a characteristic frequency; the X-rays can then be detected by the electron microprobe [4.6]. The incident electron beam has sufficient energy to liberate both matter and energy from the sample. These electron-sample interactions mainly liberate heat, but they also yield both derivative electrons and x-rays. X-ray generation is produced by inelastic collisions of the incident electrons with electrons in the inner shells of atoms in the sample; when an inner-shell electron is ejected from its orbit, leaving a vacancy, a higher-shell electron falls into this vacancy and must shed some energy (as an X-ray) to do so. These quantized x-rays are characteristic of the element. EPMA analysis is considered to be "non-destructive"; that is, x-rays generated by electron interactions do not lead to volume loss of the sample, so it is possible to re-analyze the same materials more than one time [4.7].

**EPMA consists of four major components:**

- An electron source commonly referred as a "gun."
- A series of electromagnetic lenses located in the column of the instrument, used to condense and focus the electron beam emanating from the source; this comprises the electron optics and operates in an analogous way to light optics.
- A sample chamber, with movable sample stage (X-Y-Z), that is under a vacuum to prevent gas and vapor molecules from interfering with the electron beam on its way to the sample; a light microscope allows for direct optical observation of the sample.
- A variety of detectors arranged around the sample chamber that are used to collect x-rays and electrons emitted from the sample.

**Applications**

- Quantitative EPMA analysis is the most commonly used method for chemical analysis of geological materials at small scales.
- EPMA is chosen in cases where individual phases need to be analyzed or where the material is of small size or valuable for other reasons (e.g., experimental run product, sedimentary cement, volcanic glass, matrix of a meteorite, archeological artifacts such as ceramic glazes and tools).
- In some cases, it is possible to determine a U-Th age of a mineral such as monazite without measuring isotopic ratios.

- EPMA is also widely used for analysis of synthetic materials such as optical wafers, thin films, microcircuits, semi-conductors, and superconducting ceramics.

#### **4.8. X-Ray Diffraction (XRD)**

X-ray crystallography is a method of determining the arrangement of atoms within a crystal, in which a beam of X-rays strikes a crystal and diffracts into many specific directions. From the angles and intensities of these diffracted beams, a crystallographer can produce a three-dimensional picture of the density of electrons within the crystal. From this electron density, the mean positions of the atoms in the crystal can be determined, as well as their chemical bonds, their disorder and various other information.

In an X-ray diffraction measurement, a crystal is mounted on a goniometer and gradually rotated while being bombarded with X-rays, producing a diffraction pattern of regularly spaced spots known as reflections. The two-dimensional images taken at different rotations are converted into a three-dimensional model of the density of electrons within the crystal using the mathematical method of Fourier transforms, combined with chemical data known for the sample. Poor resolution (fuzziness) or even errors may result if the crystals are too small, or not uniform enough in their internal makeup.

The X-ray diffraction (XRD) patterns of the samples annealed at various temperatures were recorded by a Rigaku diffractometer using the Cu K $\alpha$  radiation at a scanning step of 0.02°.



#### 4.9. Surface Profiler

Surface analysis and accurate surface characterizations are critical in thin film characterization. Surface profilers are used to measure surface profiles, roughness, thickness, waviness and other parameters. We used Dektak-II surface profiler for characterization of our samples. In the surface profiler a tip flows in contact with sample surface following its morphology. A position transducer converts tip movements into height values producing the surface profile. We used surface profiler to determine film thickness, sputtering rate, and band gap characterization in this thesis.



**Fig. 4.9. Surface Profiler Dektak-II**

In order to determine film thickness first we measured the substrate thickness and then sample thickness after each sputtering process, this data was used to determine sputtering rate for different materials. We measured film thickness of samples at three places in order to make results accurate. Fig. 4.9. shows the surface profiler used for sample characterization in this work.

#### **4.10. Spectrophotometer**

Fig. 4.10 shows the spectrophotometer Shimadzu MPC-3100 used for sample characterization in this thesis. We measured transmittance of pre and post annealed samples with spectrophotometer.



**Fig. 4.10. Spectrophotometer Shimadzu MPC-3100**

#### WORKS CITED

- 4.1. Yu-Ching Huang, Yu-Chia Liao, Shao-Sian Li, Ming-Chung Wu, Chun-Wei Chen, and Wei-Fang Su “Study of the effect of annealing process on the performance of P3HT/PCBM photovoltaic devices using scanning-probe microscopy” *Solar Energy Materials and Solar Cells*, vol. 93, Issues 6-7, Pages 888-892 (2009).
- 4.2. Ki-Jun Yun, Dong-Ryeol Jung, Sung-Kil Hong, Jong-Ha Moon, and Jin-Hyeok Kim, “Effects of Annealing Atmosphere on the Characteristics and Optical Properties of SiON Films Prepared Plasma Enhanced Chemical Vapor Deposition” *New Materials for Microphotonics MRS Proceedings* vol. 817, L6.13 (2004).
- 4.3. Z. Zhi, Y Qi, H Z Yang, J H Wang, X M Yu, and B S Zhang “Effects of annealing temperature on optical properties of ZnO nanocrystals embedded in SiO<sub>2</sub> matrix thin films” *J. Phys. D*: 40, 4281-4284.
- 4.4. Jong-Yoon Hal, Ji-Won Choi, Chong-Yun Kang, S. F. Karmanenko, Seok-Jin Yoon, Doo-Jin Choi, and Hyun-Jai Kim, “Effects of Annealing Process on Dielectric Properties of (Ba,Sr)TiO<sub>3</sub> Thin Films Grown by RF Magnetron Sputtering” *Jpn. J. Appl. Phys.* 44 pp. L1196-L1198 (2005).
- 4.5. Jie Liu, Tzung-Fang Guo, and Yang Yang, “Effects of thermal annealing on the performance of polymer light emitting diodes” *J. Appl. Phys.* vol. 91, no.3, (2002).
- 4.6. W. Jansen. M. Slaughter, "Elemental mapping of minerals by electron microprobe", *American Mineralogist* 67 (5-6), 521–533 (1982).
- 4.7. <http://serc.carleton.edu/>

**CHAPTER - 5**

**RESULTS AND  
DISCUSSION**

### 5.1. Results and discussion

In this section, we will present and discuss all the results we obtained from our experiments. First we will present the results of Erbium-doped silicon dioxide films ( $\text{Er-SiO}_2$ ) fabricated with RF sputtering. Fig.5.1 shows the PL spectra of  $\text{Er-SiO}_2$  films annealed at different temperatures in ambient air. As deposited samples exhibit photoluminescence centered at 620 nm wavelength. Post-annealed samples did not show photoluminescence.

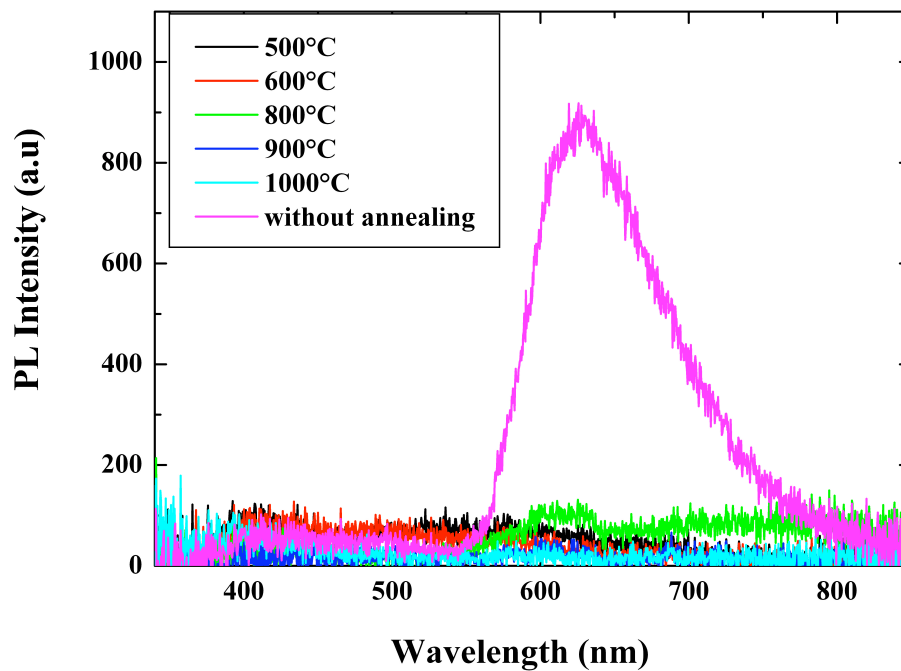


**Fig. 5.1. PL spectrum of  $\text{Er-SiO}_2$  films annealed at different temperatures**

Fig.5.2 shows the PL spectra of samples fabricated with different number of  $\text{Er}_2\text{O}_3$  tablets. Sample fabricated with two  $\text{Er}_2\text{O}_3$  tablets shows the strongest PL intensity

among all the samples. Fig.5.3 shows the PL spectra of Er-SiO<sub>2</sub> films with different film thickness. Sample with 1.84  $\mu\text{m}$  thickness shows the strongest PL intensity.

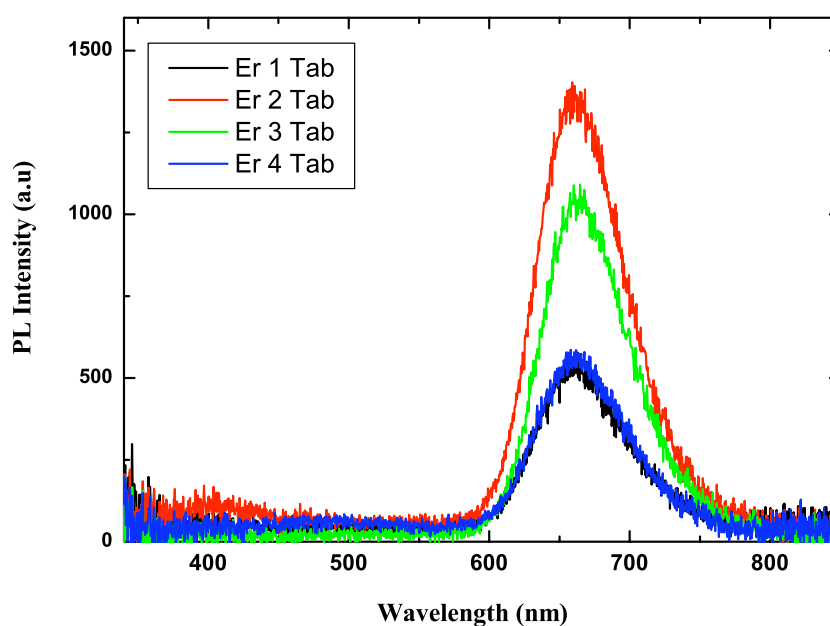


**Fig. 5.2. PL spectrum of Er-SiO<sub>2</sub> films with different Er concentration**

We observed photoluminescence at 660 nm wavelength from Er-SiO<sub>2</sub> samples. Strongest PL intensity observed from the sample fabricated with two Er<sub>2</sub>O<sub>3</sub> tablets and 2.18  $\mu\text{m}$  film thickness. Samples did not show any PL after annealing.

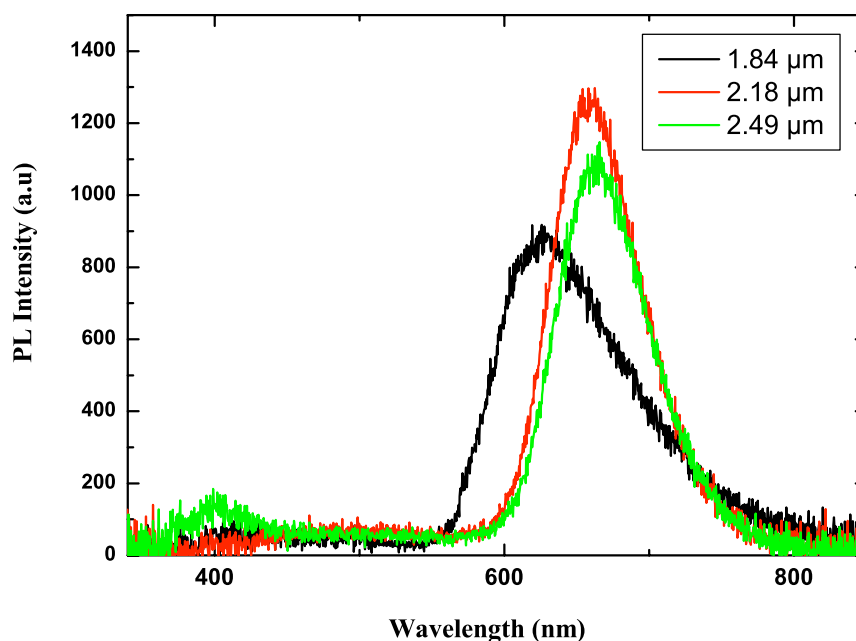


**Fig. 5.3. PL spectrum of Er-SiO<sub>2</sub> films with different film thickness**

Next we will discuss the results of Ta<sub>2</sub>O<sub>5</sub> and Er-TaO<sub>x</sub> thin films fabricated by sputtering. In order to understand light emission and optical properties of tantalum, it is important to understand band gap behavior of the tantalum thin films. In this part, we will present the results of optical band gap and absorption coefficient investigation in the tantalum thin films annealed at different temperatures.

To calculate bandgap, first we measured transmittance of the films with Shimadzu MPC-3100 Spectrophotometer. Fig.5.4 shows the transmittance spectra of samples annealed at different temperatures.

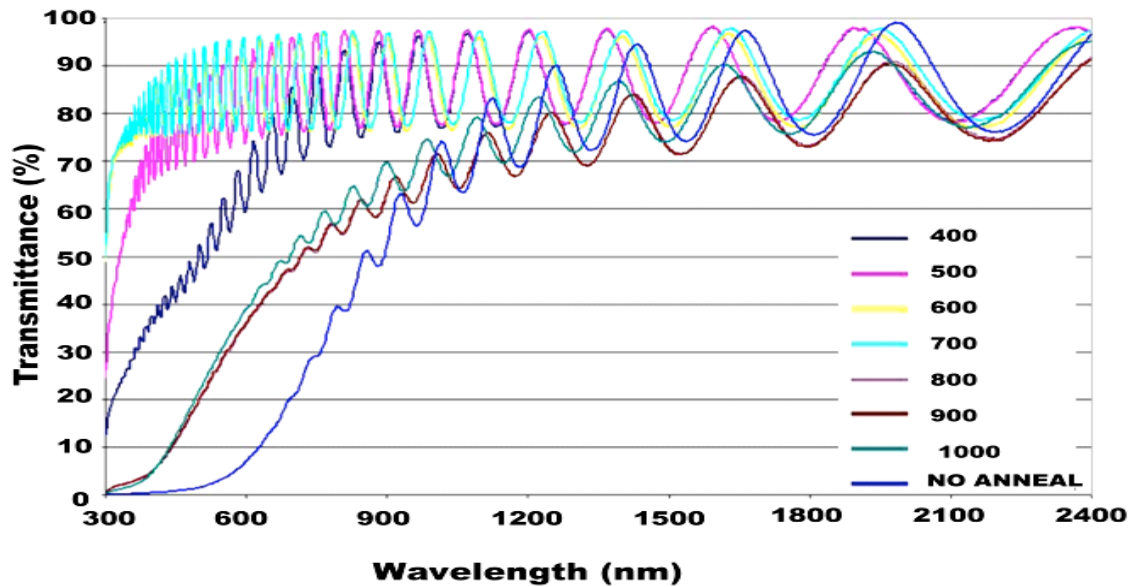


Fig. 5.4. Transmittance spectra of samples

The absorption coefficient  $\alpha$  can be calculated from the relation [5.1]

$$T = A \exp(-\alpha d) \quad \dots\dots\dots (1)$$

where, T is the transmittance of thin film, A is a constant, and d is the film thickness. Constant A is approximately unity, as the reflectivity is negligible and insignificant near the absorption edge. The optical band gap of the films is determined by applying the Tauc model [5.2] and the Davis and Mott model [5.3] in the high absorbance region

$$\alpha h\nu = D (h\nu - E_g)^n \quad \dots\dots\dots (2)$$

where  $h\nu$  is the photon energy,  $E_g$  is the optical band gap and D is a constant.  $n=2$  for direct transition materials. Fig. 5.5 shows graph between absorption coefficient and estimated band gap energy.



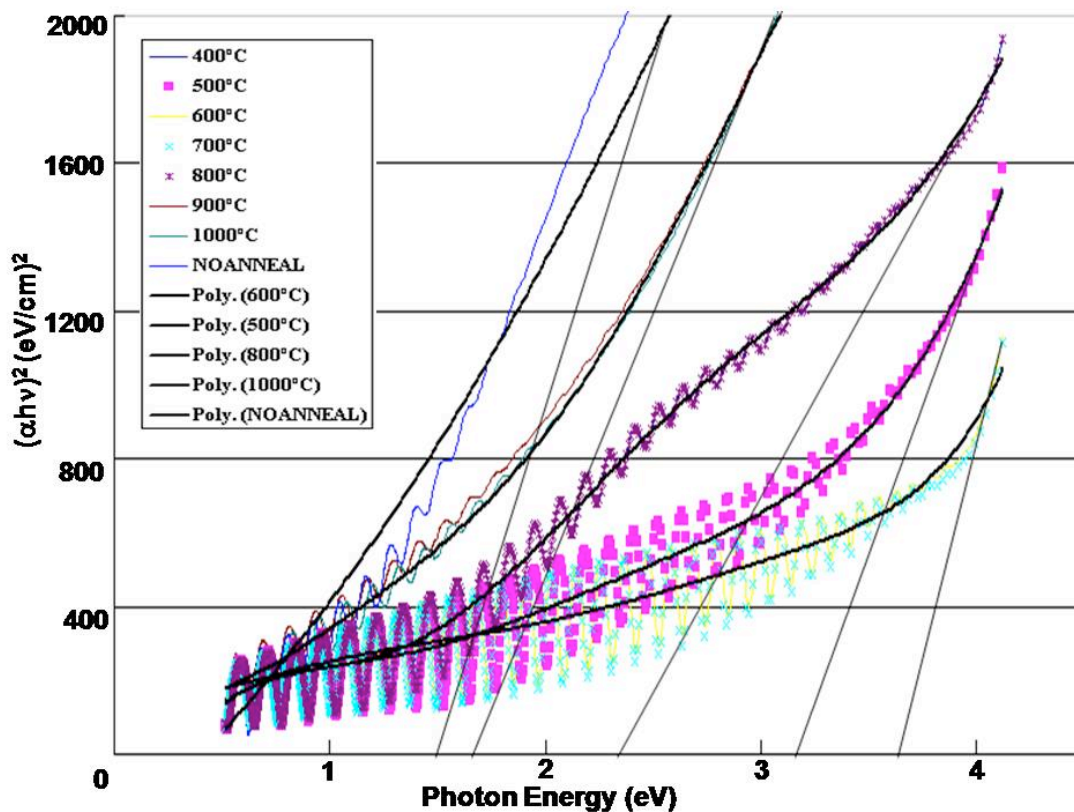


Fig. 5.5. Photon energy V/s absorption coefficient

Fig. 5.4 shows the transmittance spectra of annealed samples from 400-1000°C, In Fig. 5.5 the relationship between absorption coefficient and  $h\nu$  is plotted. The  $E_g$  value can be obtained by extrapolating the linear portion to the photon energy axis in the Fig.5.5. The optical band-gap values obtained are summarized in Table 5.1.

We noticed as the annealing temperature was decreased from 1000 to 600 °C, the optical band gap shifted from 3.7-1.6eV.

**Table -5.1. Change in bandgap with various annealing temperature**

<b>Annealing Temperature</b>	<b>Bandgap</b>
600 °C	3.7eV
700 °C	3.7eV
800 °C	2.4eV
900/1000 °C	1.6eV

We prepared the tantalum pentoxide films with RF sputtering method. We observed the lowest transmittance from the as deposited film due to their amorphous nature. After annealing, films show better transmittance, which could be because of more uniform film structure. Highest percentage of transmittance can be found in the films with annealing temperature of 600 and 700°C. Films annealed at 500°, 600° and 700°C shows a bandgap of 3.7-3.2 eV. Films annealed at 800°C, shows the bandgap of 2.4 eV. Films annealed at 900°-1000°C, shows band gap of 1.6 eV. It's difficult to determine a direct relationship between amorphous disordered thin films crystal structure and band gap behavior. After annealing, change of bandgap and transmittance of films could be due to the change of phase and crystal structure.

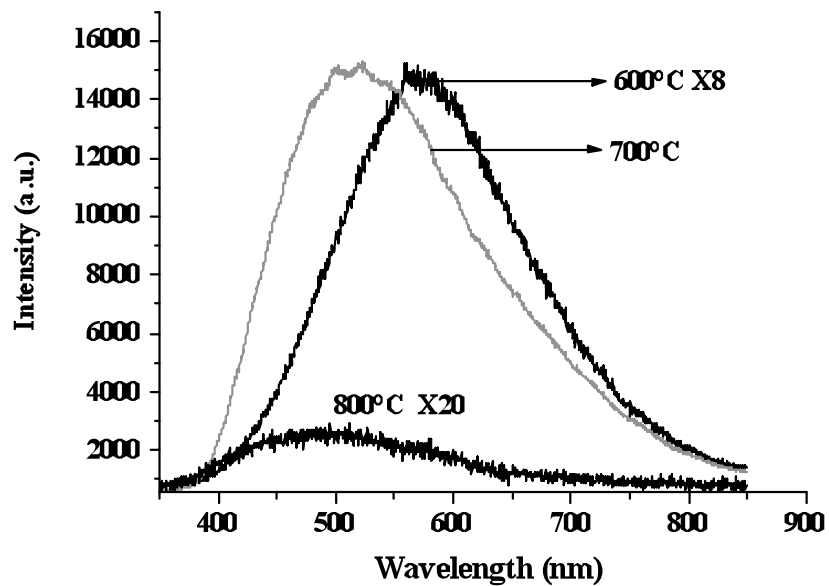


**Fig. 5.6.** PL spectra of Ta-oxide films after annealing at 600°, 700° and 800°C

Fig.5.6 shows the photoluminescence spectra of tantalum pentoxide films annealed at various temperatures. We did not observe light emission from as sputtered film. Post-annealed films show visible light emission after annealing at 700°C. Sample annealed at 700°C shows the highest PL intensity. The wavelength of photoluminescence centered around 510 nm. Miura et al. reported blue light emission from tantalum pentoxide films fabricated by RF-magnetron sputtering [5.4]. Zhu et al. reported red light emission from amorphous tantalum pentoxide films [5.5].

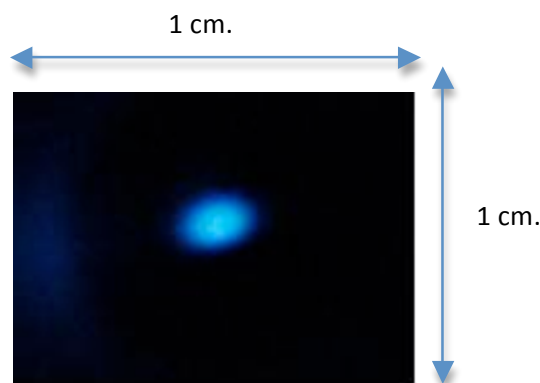


**Fig. 5.7. Visible light emission from tantalum pentoxide film annealed at 700°C**

Fig. 5.7 shows the visible light emission from tantalum pentoxide film annealed at 700°C for 20 min. We observed green light emission (wavelength 510 nm) from tantalum pentoxide films in our result, which was not reported in previous works. As far as origin of green light emission is concerned, it is not very clear yet and we are still trying to investigate the origin of green light emission.

In next step, we tried to optimize the annealing time, RF power and Ar flow rate for strong PL intensity. Samples were annealed for 20, 30, and 40 min in KDS-70 heating furnace. Fig.5.8 shows PL spectra of samples annealed for 20, 30, and 40 min. Samples annealed for 30 and 40 min show strong PL intensity.

Fig.5.9 shows PL spectra of samples fabricated with different RF power during sputtering process. Sample fabricated with 100 W RF power shows stronger PL intensity than samples fabricated with 200 and 300 W RF power.

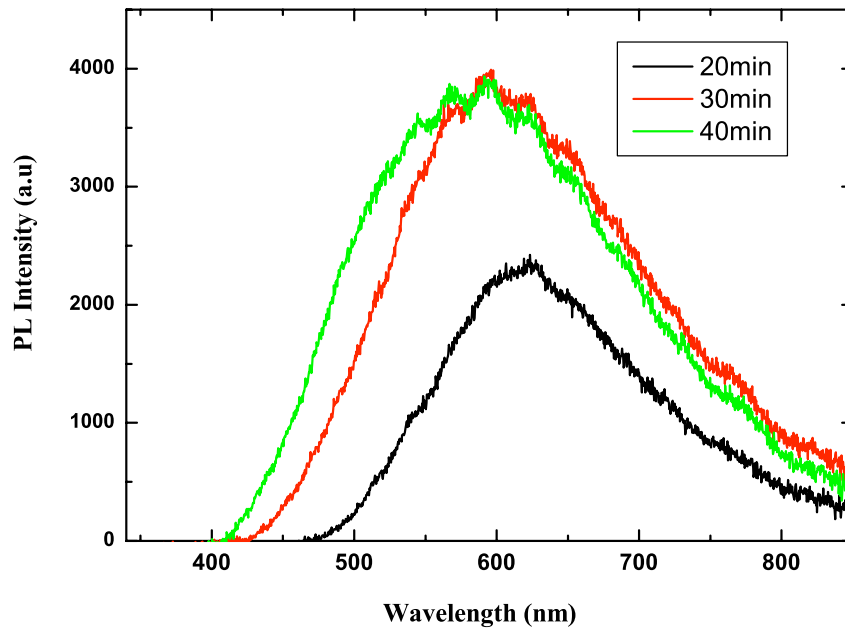


**Fig. 5.8. PL Spectra of samples annealed for 20, 30 and 40 min.**

Fig. 5.10 shows PL spectra of samples fabricated with different Ar flow rate during sputtering process. Sample fabricated at 5sccm Ar flow rate shows stronger PL intensity than samples fabricated at 10 and 15 sccm Ar flow rate.

We observed strongest PL intensity from the sample fabricated with 100 W RF power, 5 sccm Ar flow rate, and 30 min annealing time.

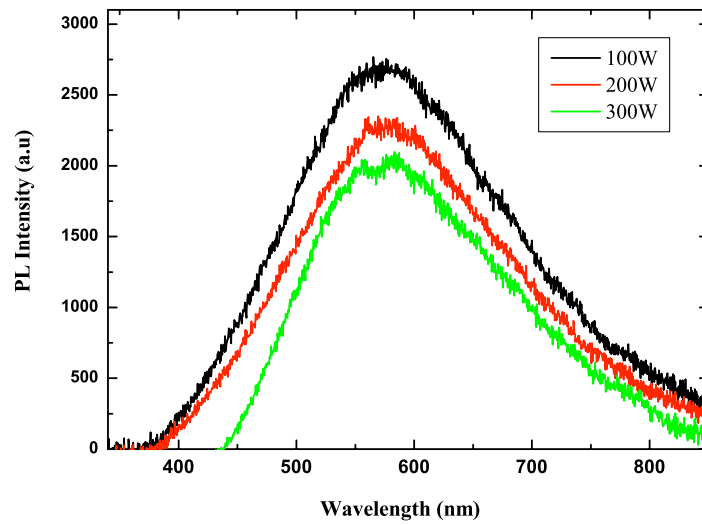


Fig. 5.9. PL spectra of samples fabricated with different RF power

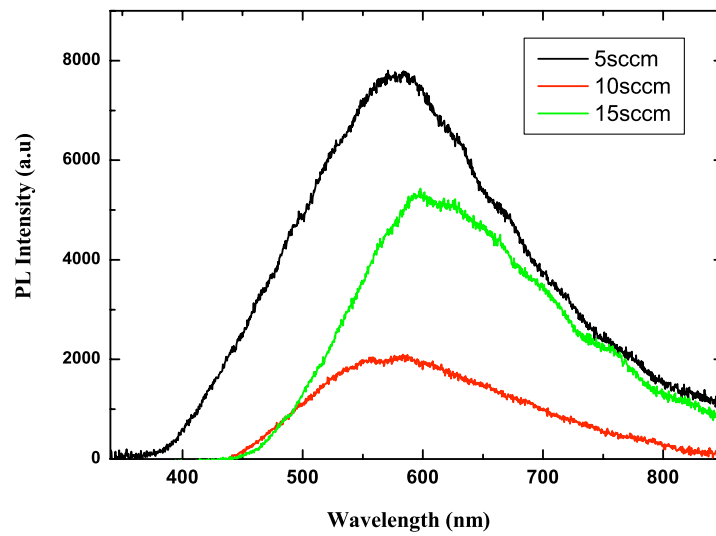


Fig. 5.10. PL spectra of samples fabricated with different Ar flow rate

### Erbium-doped Tantalum pentoxide

Fig. 5.11 plots the PL spectra of Er-TaO<sub>x</sub> films fabricated using two Er<sub>2</sub>O<sub>3</sub> tablets and annealed from 600° to 1100°C for 20 min. The as-deposited samples did not exhibit PL. We observed two PL peaks at 550 and 670 nm from post-annealed samples. The sample annealed at 900°C exhibits the strongest PL intensity. The PL peaks observed at 550 and 670 nm are due to the transitions of Er<sup>3+</sup> from the <sup>4</sup>S<sub>3/2</sub> to the <sup>4</sup>I<sub>15/2</sub> state and from the <sup>4</sup>F<sub>9/2</sub> to the <sup>4</sup>I<sub>15/2</sub> state respectively [5.6]. Light emission at 670 nm could not be observed in the samples annealed at 600° and 700°C.

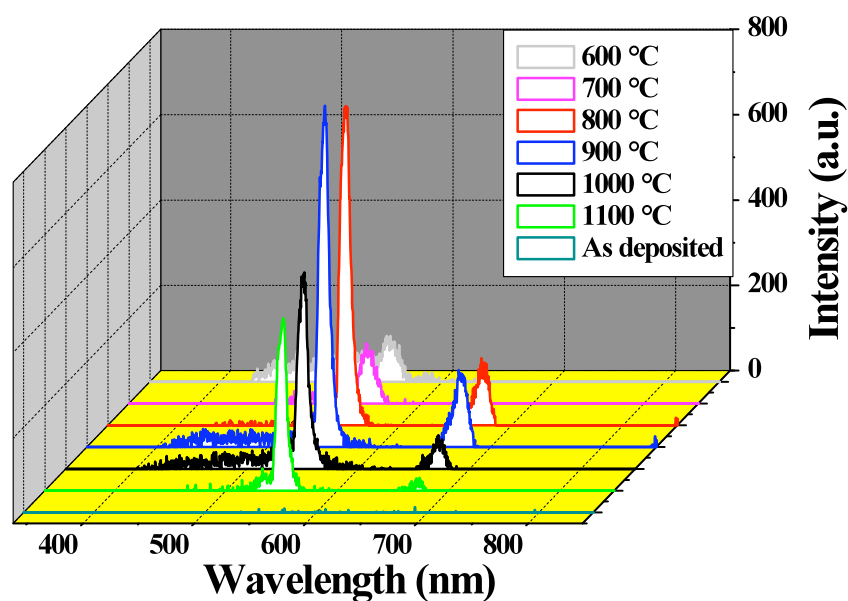


Fig. 5.11. PL spectra of Er-TaO<sub>x</sub> films annealed at 600° to 1100°C for 20 min.

## Chapter 5

### Results and Discussion

---

To observe the effect of annealing time on PL intensity and to optimize the annealing time, we annealed samples (fabricated with two  $\text{Er}_2\text{O}_3$  tablets) at  $900^\circ\text{C}$  for 10 to 40 min in ambient air. Fig. 5.12 plots the PL spectra for different annealing times. The sample annealed for 20 min had the strongest PL intensities at both wavelengths of 550 and 670 nm.

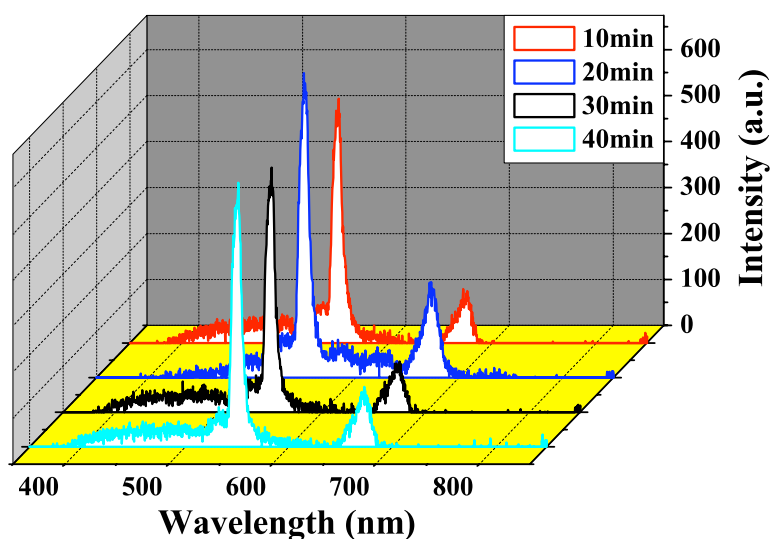


**Fig. 5.12. PL spectra of samples annealed at  $900^\circ\text{C}$  for 10 - 40 min**

Fig. 5.13. plots the PL spectra with different Er concentrations annealed at  $900^\circ\text{C}$  for 20 min. It has been reported that fluorescence due to  $\text{Er}^{3+}$  exhibits the strongest intensity at 1.2, 0.75, and 2 mol % Er concentration [5.7-5.9]. In our work, we observed the strongest PL intensity with 0.96 and 0.63 mol% Er concentrations at 550 and 670 nm, respectively. Table-5.2 shows the detailed results of Er concentrations in different samples measured with EPMA.



Table - 5.2. Concentration of Er in different samples measured with EPMA.

Number of Er <sub>2</sub> O <sub>3</sub> tablet on Ta <sub>2</sub> O <sub>5</sub> disc	1	2	3	4	5
Er concentration (mol %)	0.46	0.63	0.96	1.32	2.08

We observed an increase in Er concentration with the increasing number of Er<sub>2</sub>O<sub>3</sub> tablets on the Ta<sub>2</sub>O<sub>5</sub> disc. It appears that different fabrication methods and dissolution sites of Er in the host material affect the Er concentration required to optimally enhance the PL intensity.

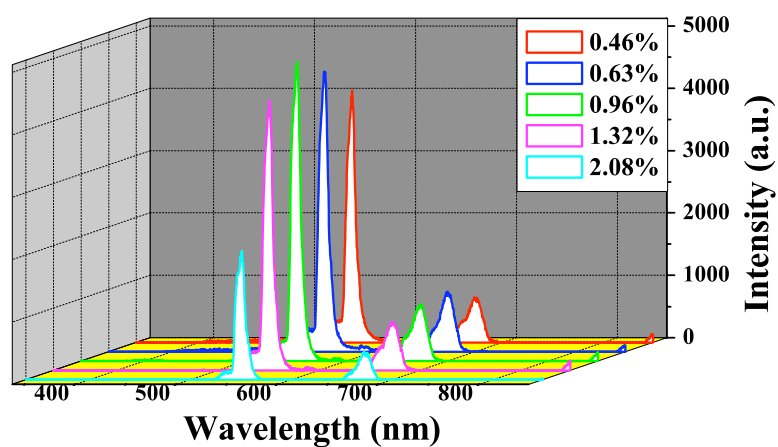


Fig. 5.13. PL spectra of samples with different Er concentrations (mol %) annealed at 900°C for 20 min.

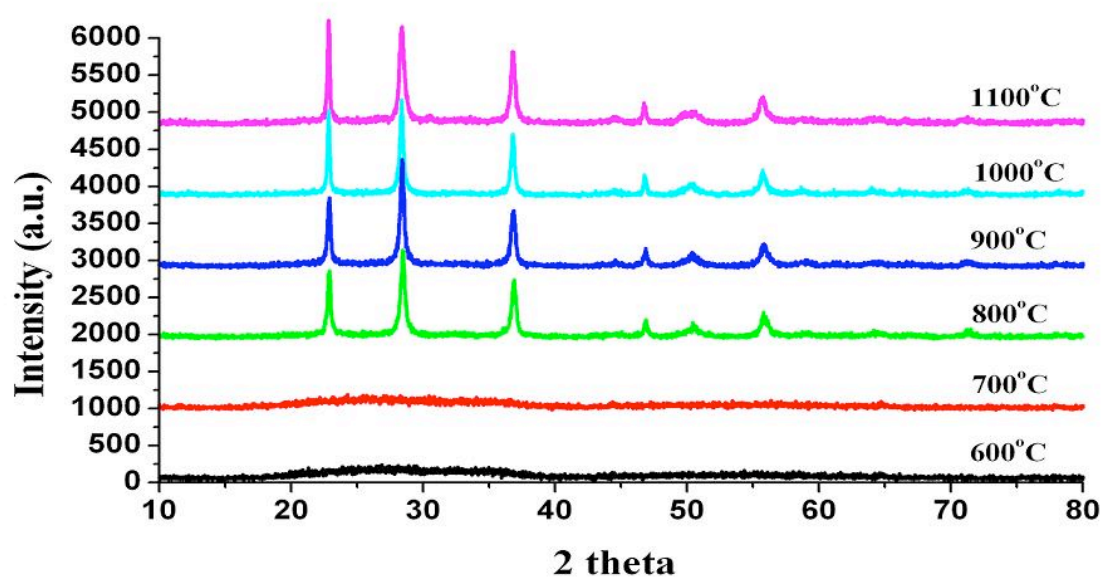


Fig. 5.14. XRD patterns of the films annealed at various temperatures.

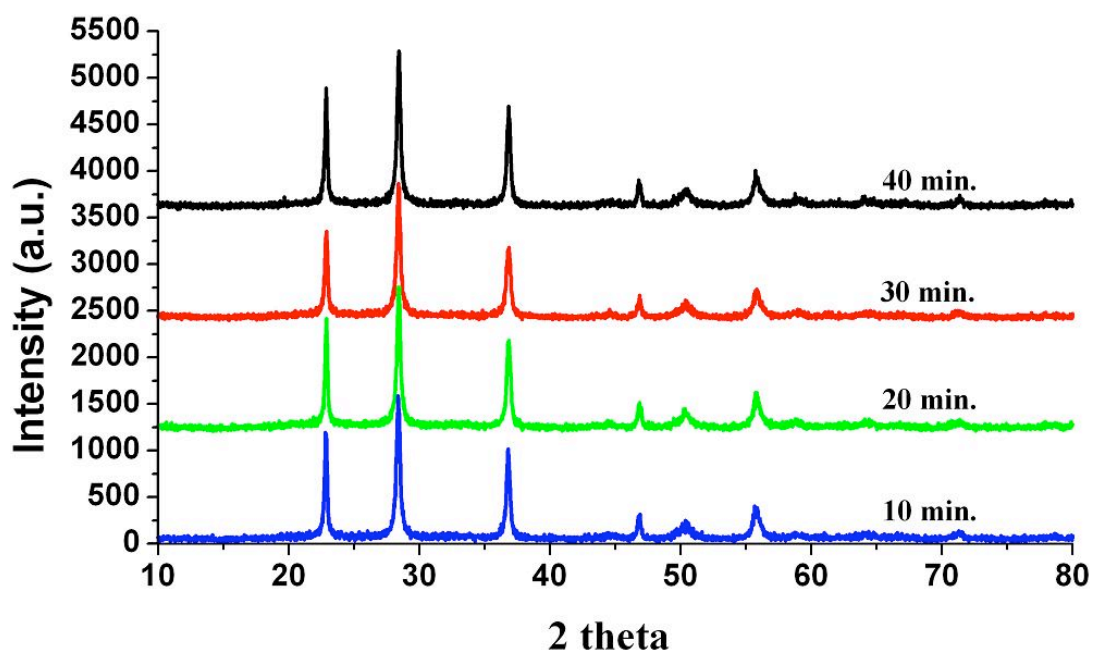
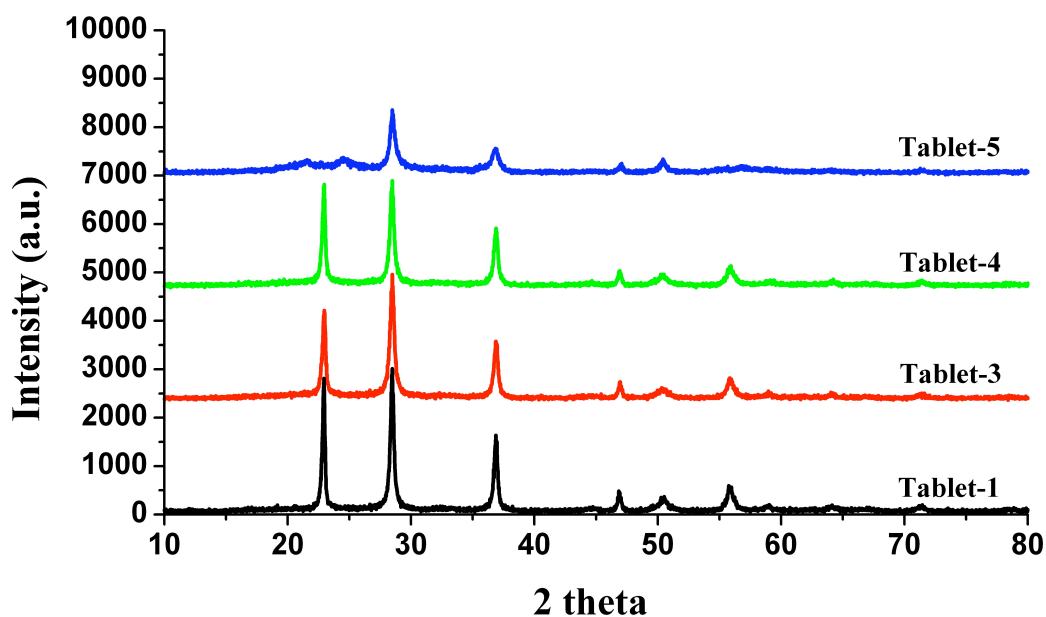


Fig. 5.15. XRD patterns of the films annealed from 10 to 40 min.



**Fig. 5.16. XRD patterns of the films fabricated with different Er concentration.**

Fig. 5.14 shows the XRD patterns of the films annealed at various temperatures. Fig. 5.15 shows the XRD patterns of the films annealed at 900°C from 10 to 40 min. Fig. 5.16 shows the XRD patterns of the films fabricated with different Er concentration.

The diffraction pattern fits well with references [5.10 and 5.11]. The absence of 2 $\theta$  peaks in samples annealed below 800°C indicates amorphous Ta<sub>2</sub>O<sub>5</sub> film formation. XRD Patterns of the sample annealed at 800° and 900°C probably show a mixed phase of  $\delta$ - Ta<sub>2</sub>O<sub>5</sub> (hexagonal, low-temperature phase) and  $\beta$ - Ta<sub>2</sub>O<sub>5</sub> (orthorhombic, high-temperature phase) [5.12]. High PL intensities in the samples annealed at 800° and 900°C could be a result of crystallization of the films. We can observe a change in intensity of the first peak ( $2\theta = 23^\circ$ ) in the samples annealed at 1000° and 1100°C.

In the samples annealed at 1000° and 1100°C,  $\beta$ - Ta<sub>2</sub>O<sub>5</sub> (orthorhombic) grew more than  $\delta$ - Ta<sub>2</sub>O<sub>5</sub> (hexagonal), therefore a change in PL intensity was observed.

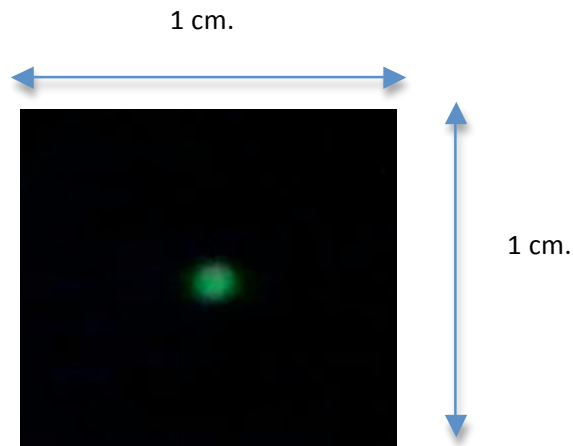


**Fig. 5.17. Green light emission from Er-TaO<sub>x</sub> films.**

As we have mentioned earlier, some previous works reported PL from Er-TaO<sub>x</sub> films. Kojima et al. [5.13] observed a green fluorescence peak around 550 nm from samples fabricated with sol-gel process. Rigneault et al. [5.14] also reported fluorescence spectra centered at 532 and 1530 nm from Er-TaO<sub>x</sub> samples fabricated with ion implantation. Maeda et al. [5.15] also reported fluorescence spectra around 550 nm and a weak peak around 660 nm with sol-gel process. In comparison to these previous works, we observed two very sharp PL peaks at 550 and 670 nm. Moreover, we observed visible green light emission by the naked eye that was not reported previously. This concludes that PL intensity at 550 nm is stronger in our results than previously reported works.

TaO<sub>x</sub> is superior to SiO<sub>2</sub> and GeO<sub>2</sub> in terms of both the phonon energy and Er<sup>3+</sup> solubility. Amorphous Ta<sub>2</sub>O<sub>5</sub> has better Er<sup>3+</sup> solubility than SiO<sub>2</sub> because of the relatively large amount of edge oxygen having a negative charge [5.9]. The crystalline bulk phase of Ta<sub>2</sub>O<sub>5</sub> is known to exist below 1630K [5.16], but its crystal structure is not uniquely determined. Processing conditions and impurities have subtle effects on

## Chapter 5

### *Results and Discussion*

---

the crystal structure and light emission. It is surmised that the change in light intensity of films after annealing is the result of changes in the phase, the crystal structure, and the dissolution site of  $\text{Er}^{3+}$  in the  $\text{Ta}_2\text{O}_5$ .

### Er-TaOx films with Ytterbium-doping

Yb is well known as a sensitizer for Er as it has larger absorption area than Er. It can absorb the energy efficiently and transfer the energy to Er, which helps to enhance Er emission at 1550 nm wavelength. Er-Yb co-doped fiber amplifiers are popular and commercially available. There is no report of energy transfer from Yb to Er at 550 and 670 nm wavelengths. We tried to observe that if transfer of energy from Yb to Er is also possible at 550 and 670 nm wavelengths, in this work.

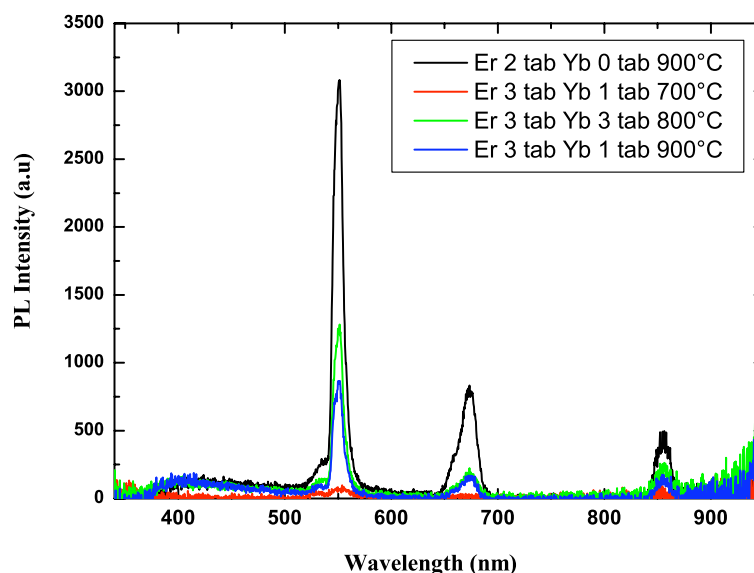


**Fig. 5.18. PL spectra of samples with different Er-Yb concentrations annealed at different temperature for 20 min.**

Fig. 5.18 shows the PL spectra of samples with different Er-Yb concentrations annealed at different temperature for 20 min. The strongest PL intensity was observed from the sample fabricated with two tablets of Er and annealed at 900°C.

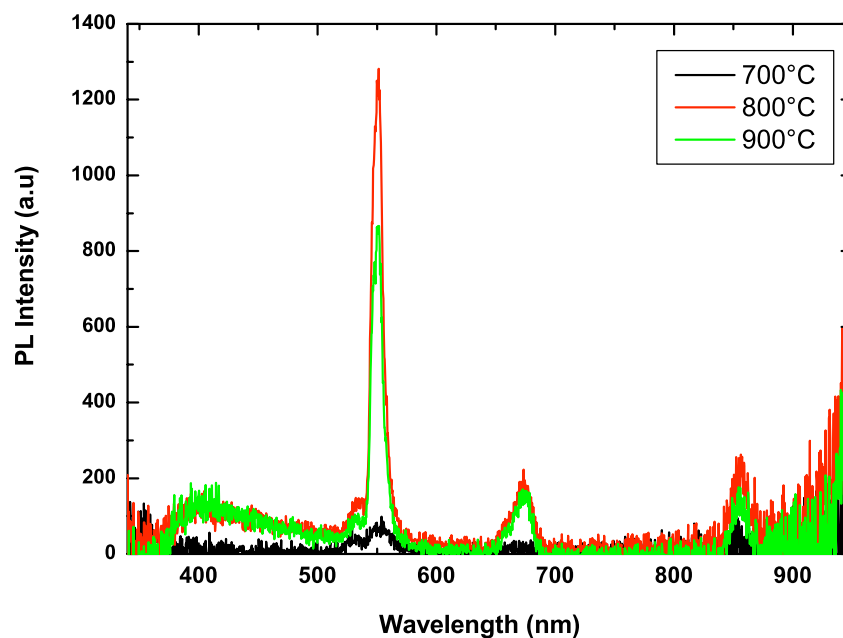


**Fig. 5.19. PL spectra of samples annealed at different temperatures for 20 min.**

Fig. 5.19 shows the PL spectra of samples annealed at different temperature for 20min. The strongest PL intensity was observed from the sample annealed at 800°C.

We did not observe any significant improvement in PL intensity at 550 and 670 nm wavelengths due to Yb doping.

**WORKS CITED**

- 5.1. E. Kim, Z. Jiang, K. No, "Measurement and calculation of optical band gap of chromium aluminum oxide films" *Jpn. J. Appl. Phys.* Vol. 394820-4825, 2000.
- 5.2. J. Tauc, *Amorphous and Liquid Semiconductors* Plenum, London, 1974.
- 5.3. A. David and N. F. Mott, *Philos. Mag.* 22, 903, 1970.
- 5.4. K. Miura, H. Miyazaki, and O. Hanaizumi, "Observation of blue-light emission from tantalum oxide films deposited by using radio-frequency magnetron sputtering," *IEICE Trans. Electron.*, vol. E91-C, no. 10, pp. 1669-1672, 2008.
- 5.5. M. Zhu, Z. Zhang, and W. Miao, "Intense photoluminescence from amorphous tantalum oxide films," *Appl. Phys. Lett.*, vol. 89, 021915, 2006.
- 5.6. E. Desurvire (ed.), *Erbium doped fiber amplifiers*, Wiley, New York, 1994
- 5.7. W. Xu, S. Dai, L. M. Toth, G. D. Del Cul, and J. R. Peterson, "Green upconversion emission from  $\text{Er}^{3+}$  ion doped into sol-gel silica glasses under red light (647.1 nm) excitation," *J. Phys. Chem.*, vol. 99, no. 13, pp. 4447-4450, 1995.
- 5.8. Y-L. Lu, Y-Q. Lu, and N-B. Ming, "Fluorescence and attenuation properties of  $\text{Er}^{3+}$ -doped phosphate-glass fibers and efficient infrared-to-visible up-conversion," *Appl. Phys. B*, vol. 62, no. 3, pp. 287-291, Mar. 1996.
- 5.9. A. Kishimoto, H. Sugimoto, T. Namba, and T. Kudo, "The influence of internal stress on the amorphous structure of wet-coated films derived from peroxopolytantalate solution," *Thin Solid Films*, vol. 204, no. 1, pp. L5-L8, Sep. 1991.
- 5.10. JCPDS No.00-025-0922, PDF2, International center for diffraction data: Newton square, PA.
- 5.11. S. J. Wu, B. Houg, B. Huang, "Effect of growth and annealing temperatures on crystallization of tantalum pentoxide film prepared by RF magnetron sputtering method," *J. Alloy. Compd.*, vol. 475, no. 1-2, pp. 488-493, 2009.



## Chapter 5

### *Results and Discussion*

---

- 5.12. N. Inoue, T. Ninomiya, S. Kashiwabara, and R. Fujimoto, "Ta<sub>2</sub>O<sub>5</sub> thin-films deposited by off-axis and on-axis pulsed laser deposition techniques," *Appl. Phys. A*, vol. 69, Supplement 1, pp. S609-S612, 1999.
- 5.13. K. Kojima, S. Yoshida, and H. Shiraishi, "Green upconversion fluorescence in Er<sup>3+</sup>-doped Ta<sub>2</sub>O<sub>5</sub> heated gel," *Appl. Phys. Lett.*, vol. 67, no. 23, pp. 3423-3425, 1995.
- 5.14. H. Rigneault, F. Flory, S. Monneret, S. Robert, and L. Roux, "Fluorescence of thin films doped by kilo-electron-volt Er implantation: application to microcavities," *Appl. Opt.*, vol. 35, no. 25, pp. 5005-5012, 1995.
- 5.15. N. Maeda, N. Wada, H. Onoda, A. Maegawa, and K. Kojima, "Preparation and optical properties of sol-gel derived Er<sup>3+</sup> doped Al<sub>2</sub>O<sub>3</sub>-Ta<sub>2</sub>O<sub>5</sub> films," *Opt. Mater.*, vol. 27, no. 12, pp. 1851-1858, 2005.
- 5.16. N. C. Stephenson and R. S. Roth, "Structural systematics in the binary system Ta<sub>2</sub>O<sub>5</sub>-WO<sub>3</sub>. V. The structure of the low-temperature form of tantalum oxide L-Ta<sub>2</sub>O<sub>5</sub>," *Acta Crystallog. Sect. B*, vol. 27, no. 5, pp. 1037-1044, 1971.

**CHAPTER - 6**

**SUMMARY AND  
CONCLUSION**

### **6.1. Summary and Conclusion**

We fabricated functional thin films with different materials and optimized the fabrication and annealing condition for light emission. We observed PL at different wavelengths due to different materials, fabrication method and annealing conditions. These are the main findings of this dissertation-

Er-SiO<sub>2</sub> films fabricated with RF sputtering show the photoluminescence centered at 620 nm wavelength. Post-annealed samples did not show photoluminescence. Strongest PL intensity was observed from the sample fabricated with two Er<sub>2</sub>O<sub>3</sub> tablets and 2.18μm film thickness.

Ta<sub>2</sub>O<sub>5</sub> films show the photoluminescence spectra after annealing. We did not observe light emission from as sputtered film. Post-annealed films show visible light emission after annealing at 700°C. Sample annealed at 700°C shows the highest PL intensity. The wavelength of photoluminescence centered around 510 nm.

We fabricated Er-TaO<sub>x</sub> films using the RF-sputtering method and then annealed them at various temperatures and time durations. PL peaks were observed at wavelengths of 550 and 670 nm. We observed the strongest intensities of the 550 and 670 nm peaks from the samples with 0.96 and 0.63 mol% Er concentrations after annealing at 900°C for 20 min, respectively. δ-Ta<sub>2</sub>O<sub>5</sub> (hexagonal, low-temperature phase) is the most suitable for light emission. To the best of our knowledge, this is the first report of visible light emission observed by naked eyes from Er-TaO<sub>x</sub> films fabricated by the RF-sputtering method. These results demonstrate that Er-TaO<sub>x</sub> films fabricated by RF sputtering can serve as high-quality luminescent layers. These can easily be combined with other passive devices to realize novel active devices (e.g., a green-light-emitting

## Chapter 6

### *Summary and Conclusion*

---

photonic crystal), as only sputtering and annealing processes are needed for fabrication.

We investigated effect of Yb-doping in Er-TaO<sub>x</sub> films. No significant improvement has been observed in light intensity after Yb-doping. We observed new PL peaks in Yb-doped samples at 850 and 980 nm wavelengths.

Some other researchers also recently reported interesting optical properties from TaO<sub>x</sub> and Er-TaO<sub>x</sub> films, such as-

- TaO<sub>x</sub> films have very high third order nonlinear susceptibility  $2 \times 10^{-13}$  esu, at 1550 nm.
- Er-TaO<sub>x</sub> planer waveguide show 0.4 dB/cm loss at 1550 nm.

Such optical properties make Er-TaO<sub>x</sub> films very suitable for applications in integrated optics, as-

- **Light emitting devices**
- **Waveguides**
- **Optical switches**
- **Optical interconnects**

Results of this dissertation can be used to realize such novel photonic devices for various applications.